

UNIVERSITY OF MELBOURNE

MASTER'S THESIS

Implementing Cellular Remodelling in Discrete Cell Models

Author:

Reuben VAN AMMERS

Supervisor:

Dr. James OSBORNE

*A thesis submitted in fulfillment of the requirements
for the degree of Master of Science*

in the

School of Mathematics and Statistics

October 2017

Examiner's Copy

Declaration of Authorship

I, Reuben VAN AMMERS, declare that this thesis titled, “Implementing Cellular Remodelling in Discrete Cell Models” and the work presented in it are my own. I confirm that:

- This work was done wholly or mainly while in candidature for a research degree at this University.
- Where any part of this thesis has previously been submitted for a degree or any other qualification at this University or any other institution, this has been clearly stated.
- Where I have consulted the published work of others, this is always clearly attributed.
- Where I have quoted from the work of others, the source is always given. With the exception of such quotations, this thesis is entirely my own work.
- I have acknowledged all main sources of help.
- Where the thesis is based on work done by myself jointly with others, I have made clear exactly what was done by others and what I have contributed myself.

Signed:

Date:

“For every complex problem there’s a simple solution, and it’s wrong.”

Umberto Eco, *Foucault’s Pendulum*

UNIVERSITY OF MELBOURNE

Abstract

Faculty of Science

School of Mathematics and Statistics

Master of Science

Implementing Cellular Remodelling in Discrete Cell Models

by Reuben VAN AMMERS

Epithelial monolayers, layers of tissue in the body one cell thick, have a large impact in many biological processes. Recently, it has been seen that in response to mechanical forces, monolayers often display non-elastic properties, particularly with responses displaying multiple distinct timescales due to cellular remodelling. Current discrete cell models, which are based on static parameters, do not exhibit these properties, and so we introduce a dynamic reference state in cell centre and cell vertex models in order to represent remodelling. Using this reference state, in appropriate parameter regimes, we find that we can observe the presence of multiple timescales and the desired mechanical properties of the discrete cells as a monolayer.

Acknowledgements

I would like to thank my supervisor, Dr. James Osborne, for his tireless support, direction and feedback throughout the course of my research project. I would also like to thank my fellow Masters students, who made the two years of the Master's degree greatly enjoyable.

Contents

Declaration of Authorship	iii
Abstract	vii
Acknowledgements	ix
1 Introduction	1
1.1 Experimental Results and the Presence of Multiple Timescales	1
1.2 Cellular Remodelling	3
1.3 Overview of Thesis	5
2 Computational Models	7
2.1 Continuous Models	7
2.2 Discrete Models	8
2.2.1 Lattice Models	8
2.2.2 Cell Centre Models	10
2.2.3 Vertex Models	13
2.3 Further Models	16
2.4 Summary	17
3 Cell Centre Models	19
3.1 Evolving Reference State	19
3.2 Creep Response & Stress Relaxation Experiment	22
3.2.1 Creep	22
3.2.2 Stress Relaxation	22
3.3 Multiple Timescales	23
3.3.1 Timescale Metric	25
3.3.2 Behaviour of the System Without Remodelling	26
3.4 The Effect of Remodelling Ratio and Remodelling Rate on Time Scales	27
3.4.1 Creep Experiment	28
3.4.2 Stress Relaxation Experiment	32
3.5 The Addition of Memory Leads to Multiple Time Scales of Remodelling	35
3.6 Summary	39

4 Vertex Models	41
4.1 Implementing the Reference State	41
4.2 Choice of Potential	42
4.3 Creep Experiment - Testing Setup	45
4.4 Interaction Between States in Creep Experiment	46
4.5 Synchronising Area and Circumference	47
4.6 Cell Directionality	51
4.7 Directionality with Reference State	53
4.8 Vertex Timescales	55
4.9 Summary	57
5 Discussion & Conclusion	59
5.1 Discussion	59
5.1.1 Overview	59
5.1.2 Computational Overhead	60
5.2 Future Work	61
5.2.1 Application to Other Discrete Models	61
5.2.2 Complex System Simulation	62
5.2.3 Monolayer Restructuring with Reference State	62
5.2.4 Multiple Reference States	63
5.3 Conclusion	63
A Numerical Calculation of Forces in the Vertex Model	65
B Implementation Details of Creep and Stress Relaxation Experiments	69
C Defining Two Timescaled Behaviour	71
C.1 Suitability of Stretched Exponential Fits	71
C.2 Choice of Metric	72
D Equilibration Time Calculation	73
E Use of MATLAB Solvers for the Solution of ODEs	75
F Code	77
Bibliography	79

Chapter 1

Introduction

On the surfaces of many cavities and organs in the human and animal body, there exist many epithelial sheets of cells [22]. Many of these layers of epithelial cells are “simple”, being one cell layer thick, and are called *monolayers*. These monolayers are often subjected to mechanical forces, and therefore understanding how these cells react in the face of these forces is paramount in understanding these phenomena. Cell proliferation in the intestinal crypt produces forces which result in cell migration [10]. Inside the lung, pulmonary alveoli deform due to changing pressures during breathing, causing deformation of the one cell thick alveoli [34]. Monolayers are subjected to various forces during embryonic development, influencing morphogenesis [33]. To understand these systems better, we want to explore how these monolayers behave experimentally, and ultimately to be able to reproduce these properties computationally to perform *in silico* experiments.

1.1 Experimental Results and the Presence of Multiple Timescales

In 2011, Harris et al. [16] investigated experimentally the mechanical properties of an epithelial monolayer. To do this, they connected the edges of a cell monolayer to a set of rods, one of which was held fixed, and the other one which could be moved. Using these two rods, a variety of mechanical experiments were undertaken, where forces were applied to the dynamic rod and the resulting behaviour of the monolayer was recorded.

These monolayers at equilibrium were around 1mm in length and height, meaning that each of the monolayers experimented upon were only a few hundred cells long and high. This is a relatively small amount of cells, meaning that the small scale behaviour of these monolayers could be investigated.

A variety of different experiments were presented in this paper, but we will focus on two of them: the creep experiment and the stress relaxation experiment, as these are two of the most critical experiments in categorising the behaviour of viscoelastic materials.

In the creep experiment, the left side of the monolayer is held fixed, while the right side of the monolayer has a constant force applied to the rod attached to the monolayer, stretching the monolayer. The length of the monolayer is then recorded, and the strain, the resultant length divided by the initial length, is recorded over time.

In the stress relaxation experiment, the monolayer is pulled to the right at a constant rate and then held. The resulting force to the left, the stress, is then recorded over time.

In the resulting curves obtained from these experiments, we see the distinct presence of multiple timescales, where the monolayer produces clearly different behaviour at different times. In the creep experiment (Figure 1.1), the monolayer rapidly extends initially, followed by a slow increase in length as the applied force is maintained. The effect of this becomes more prominent as the force applied to the monolayer is increased.

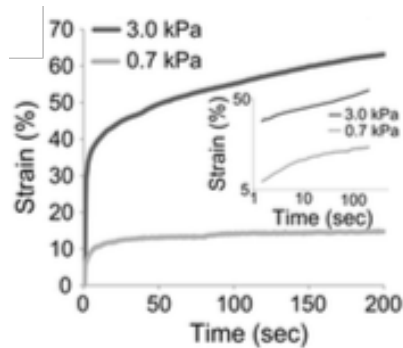
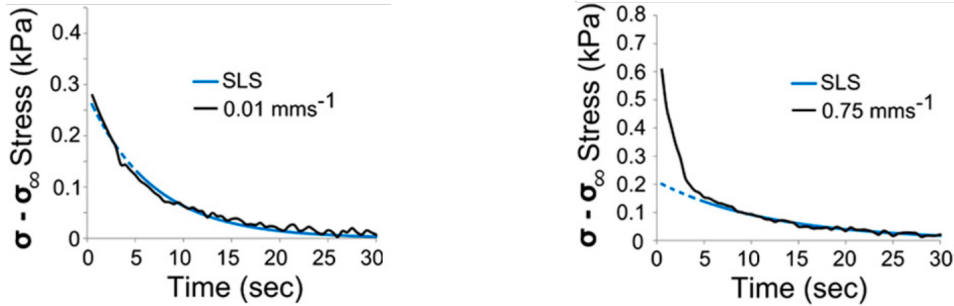


FIGURE 1.1: Strain vs time of a biological monolayer in response to external stress. Figure reproduced from Harris et al. [16].

In the stress relaxation experiment (Figure 1.2), we also see differing behaviour of the resulting stress-time curves in response to different magnitudes of external influence, in this case the strain-rate of loading. Slow initial loading produces stress-time graphs that can be accurately described as exponential behaviour. On the other hand, after high strain-rate loading, we initially see a relatively quick drop off in stress, followed by a slow decrease as time increases.



(A) Stress-time graph following high strain-rate loading. (B) Stress-time graph following low strain-rate loading.

FIGURE 1.2: Stress vs time of a stress relaxation experiment. Figures reproduced from Harris et al. [16]

In standard models of viscoelastic materials, such as the standard linear solid (SLS) model, we expect the creep and stress relaxation responses to follow exponential behaviour [12]. The deviation of these responses from simple mechanical models, despite the inherent simplicity of a monolayer compared to other biological tissue, suggest that something more complicated is in play. In tissue over a long period of time with nutrients available, one might surmise that the increase in strain is due to cell growth, or the movement of cells within the monolayer in order to react to the mechanical forces. However neither of these processes were observed in the above experiment.

Therefore, we understand that all of the change in behaviour of the monolayer occurs on an individual cellular level, and not a macroscopic holistic level. To understand this, we first have a brief look at cellular remodelling, the ability for cells to change shape, especially in response to external forces.

1.2 Cellular Remodelling

In cells, the main component responsible for their shape is the *cytoskeleton* [22]. The cytoskeleton is comprised of many different components, whose properties combine to produce of the overall qualities of the cytoskeleton. These main components are *actin*, *microtubules* and *intermediate filaments*.

Actin is a protein, and one of the most common ones within cells. Actin subunits are found throughout the cell, and can attach together, one after the other, to form actin filaments, alternatively named microfilaments. These microfilaments connect together in large structures to form the actin cytoskeleton. In order to change cell shape, these microfilaments can attach or disconnect from each other, changing the

shape of the cytoskeleton. Alternately, the individual actin filaments can depolymerise into the constituent actin subunits, and potentially polymerise elsewhere as needed. These effects are very common, being one of the main effects of cell remodelling [22].

Intermediate filaments can be made from a variety of different proteins, most notably keratins in epithelial cells. These intermediate filaments can connect together to form an intermediate filament cytoskeleton, similar to actin. In contrast to actin, intermediate filaments are relatively stable, with little polymerisation or depolymerisation of intermediate filaments occurring compared to actin, although these events do happen. Intermediate filaments can be connected to other intermediate filaments, other cytoskeletal elements or other parts of the cell via intermediate filament associated proteins [22].

Finally, microtubules are comprised of subunits of the protein tubulin. These sub-units are formed into cylinders, usually with 13 subunits in each layer of the tube. Microtubules typically radiate outwards from the centrosome, where microtubules are organised, in order to provide structure to the cell. These microtubules can disassemble and reassemble into their constituent proteins in order to facilitate cellular remodelling, with disassembly being much faster than assembly [22].

This is just an extremely brief summary of the cytoskeleton, with there being multiple other components in the cell to provide cell structure, in order to provide motility for these cytoskeletal components, or accelerate/inhibit the polymerisation/depolymerisation of filaments or microtubules. The exact nature of all of these different components is still an area of active research due to the complexity of the topic.

The important thing to note from this overview is that the cell is a very complex structure, with the relatively simple property of the shape of the cell being comprised of a huge number of different components and processes. These processes occur over different lengths of time based upon their chemical components, explaining the presence of differing properties of the cell monolayer as seen in in Section 1.1.

1.3 Overview of Thesis

Due to the inherent complexity of these processes comprising cellular remodelling, it would be an extremely daunting task to model all of these differing components exactly, especially in a way that it is computationally feasible to model aggregates of hundreds or thousands of such cells in a monolayer. However, we can attempt to model the presence of the multiple timescales observed via the addition of extra components to existing cell models in order to simulate the presence of slower intracellular phenomena.

This thesis is structured as follows. We will start in Chapter 2 by producing a brief overview of existing models for computing the behaviour of cells, and an analysis of their applicability to simulating this phenomenon, in order to see which models might be fruitfully modified in an attempt to observe the desired properties.

We will follow this in Chapter 3 by implementing the presence of cellular remodelling in the simple cell centre linear spring model, and analysing the potential behaviour of the model for emergence of multiple timescales. We will do this by adding a “reference frame” to our model to allow the presence of slower cellular processes.

Following this, in Chapter 4, we will use similar ideas to implement these effects in a more complex cell vertex model, via the addition of a reference state. The effects of and suitability for such a construction will be explored for a variety of differing implementations.

This will be capped off in Chapter 5 with a comparison between the effects of the different versions of the updated models, their suitability to be used in real simulations explored, and future work to further explore this avenue of research.

A set of appendices is also included, which generally describe numerical details or implementations that may be relevant for anyone attempting to replicate or extend this work.

Chapter 2

Computational Models

Many different mathematical formulations have been proposed to model the behaviour of biological systems. Due to the complexity of such systems, these models are not exact descriptors of the behaviour of a tissue; any sufficiently complicated model to describe the system exactly would be so involved as to be useless. Therefore, there have been many different models that focus on different aspects of the biology, trading off model accuracy for tractability as appropriate.

Resultantly, there are a huge variety of different models, using wildly different assumptions. Certain models may be appropriate for some situations, but inappropriate for others, even when modelling similar tissues, depending on what factors are being included and the nature of what is being investigated. This chapter will involve a brief overview of some of the more common models, and an analysis of the suitability to our problem of modelling multiple timescales.

2.1 Continuous Models

One of the most common descriptions of tissue is the continuous based description, where tissue is modelled as a volume subjected to a variety of different effects based upon physical laws, and the resultant behaviour is observed. The behaviour of the entire tissue is modelled in this manner, which can allow for quite accurate computations of macroscale behaviour, but one cannot look at the constituent parts of the model and see, for example, the presence of components such as cells.

The basic idea behind these continuum descriptions involves deforming tissue via the change in reference frame, from an original frame to new one. For example, simple translational motion can be described by moving every point by a constant amount. In general, the mechanical response of tissue can be described by combinations of translational, rotational and deformational tensors [4].

The response of objects to forces will be dependent on the properties of the material. For example, elastic materials will oppose stress linearly with their extension, while others will undergo permanent plastic deformation in response to external forces. Fluids on the other hand will behave very differently from either, easily deforming in response to mechanical forces and having the ability to flow.

In the body, there are many different components, all of which will have distinct properties. In order to accurately model these tissues, all of these different components need to be taken into account. The effects of these is usually captured in the mixture model, where the different components of the cell are assumed make up some proportion of total amount of cell tissue. Conservation laws, such as those of mass and momentum, then can be used to combine the effects of each of these phases for a total description of the system [20]. Further non-mechanical effects, such as tissue growth, can also be implemented into these models to take into account a wider variety of different effects [14].

These models usually result in partial differential equations that describe the nature of the system, in concert with boundary conditions. Although these may be able to be solved analytically for simple systems, usually the complexity of these will require them to be solved numerically.

By ignoring the microstructure of the body, these continuum based approaches allow behaviour of the system to be calculated which would be infeasible by taking into account the presence and location of every single cell.

2.2 Discrete Models

Although continuous based models are often good at describing effects over large regions of tissue, they don't allow the presence of individual cell effects to be observed. This may be relevant for small groups of cells, or when a more in depth explanation of effects such as mitosis needs to be modelled. In addition, many of the processes in the body are often nonlinear and the large scale superposition of processes may not necessarily be a sound assumption [4].

Therefore, there are many models which attempt to describe the behaviour of biological material from a comparatively more reductionist perspective, describing individual cells rather than tissue as a whole.

2.2.1 Lattice Models

Some of the earliest and simplest methods for describing tissue behaviour were lattice based, confining cells to be at certain locations on a predefined grid, often square or hexagonal, however other grids, such as random grids, have been used

[21]. The idea of using cellular automata to study the self replication of individual agents to observe larger scale behaviour was introduced by John von Neumann and Stanislaw Ulam [41]. Their idea was to consider a set of automata awash in a sea of components (which we can think of as nutrients from a biological perspective) which move and reproduce according to their surroundings.

Probably the most well known of these, although not the most useful one from a biological modelling perspective, is Conway's Game of Life [13], which involves a few simple rules for cells to survive, die or reproduce based upon the number of its immediate neighbours. This model, like most cellular automata models, discretises time as well as space, with each time step applying the given rules for the cellular automata simultaneously, although this doesn't necessarily need to be the case.

Due to their relative simplicity and ability to model birth processes of individual cells, they have been especially successful in tumour modelling [9, 31]. Usually, in these types of models, cells are differentiated into healthy and tumorous cells, with different laws for proliferation between the two cell types. The cells can divide due to sufficient presence of nutrients, presence of surrounding cells or other factors, allowing the growth of different types of tissue.

Another type of lattice model is the cellular Potts model, based on the Potts model from physics [15]. This uses an energy based approach, allowing a Hamiltonian to be constructed based upon the configuration of cells, for example energy based upon adhesion between different cell types.

This energy can then be used to calculate the movement of cells by a stochastic Metropolis algorithm, where trial choices are randomly made and then kept with a probability based upon the change to the Hamiltonian. The addition of an energy component to these lattice based models effectively allows one to add the presence of as many effects as wanted into the formulation of the behaviour of the system, in contrast with the relatively simple rules usually used in cellular automata. However, as is often the case, this complexity is a double edged sword, with the requirements of calculating the energy change after each move being quite computationally expensive. Therefore, these systems are usually most effective with a relatively small lattice.

The cellular Potts model has been used successfully to simulate scenarios such as morphogenesis [19] and tumour growth [40].

These lattice based models however, are inherently constrained by their simplicity. Having a cell's location being restricted to certain points prevents more complicated configurations of cells to occur, and prevents the cells from accurately responding to mechanical forces. In addition, working around their inherent locality can produce non-physical side effects. For example, cell birth at an already occupied site can involve moving a large amount of adjacent cells in order to make room [9].

Due to these problems, alternative methods for modelling discrete cells have been developed, removing the limitation that cells must be restricted to certain locations. These models are known as *off lattice models*.

2.2.2 Cell Centre Models

In cell centre models, the positions of cells are described by singular points in space, the centres of the cells. Unlike the cellular automata, they are not fixed to a lattice, and force laws describe their evolution over time as opposed to rules pertaining to lattice points. There are a variety of different choices that can be made in regards to these cell centre models, but principally comprise of defining the connectivity between the cells, and how the resulting connected cells interact with each other [32]. Many of these models for epithelial tissues use a two dimensional planar setting, assuming all of the cells and corresponding forces are coplanar, while others can be extended to three dimensions. As our setting involves monolayers, we will be focusing on the two dimensional aspects.

These cell centre based models have been used, for example, in the modelling of cell migration in the intestinal crypt [23] and in tumour modelling [37].

One common way of defining connectivity is the overlapping spheres model [20]. In this scenario, cells are given a “sphere” of influence, with all the cells whose own spheres overlap with the spheres in question are defined as being connected (Figure 2.1a). Although the name might suggest otherwise, other shapes such as ellipsoids or polyhedra may be used in lieu of the sphere in order to define connectivity. Different cells may be represented by different shapes or sizes as appropriate.

The other most common way of defining the connectivity between cells is by a triangulation method. In this case, at the start of simulations, the cell centre’s locations are used as vertices in a triangulation of the domain. The triangulation method used is often a Delaunay triangulation [6]. With this method of connectivity, the edges of the triangles between cells define the connectivity between cells (Figure 2.1b). The connectivity between cells can be potentially updated appropriately in response to forces or cell events such as birth, depending on the cell model used.

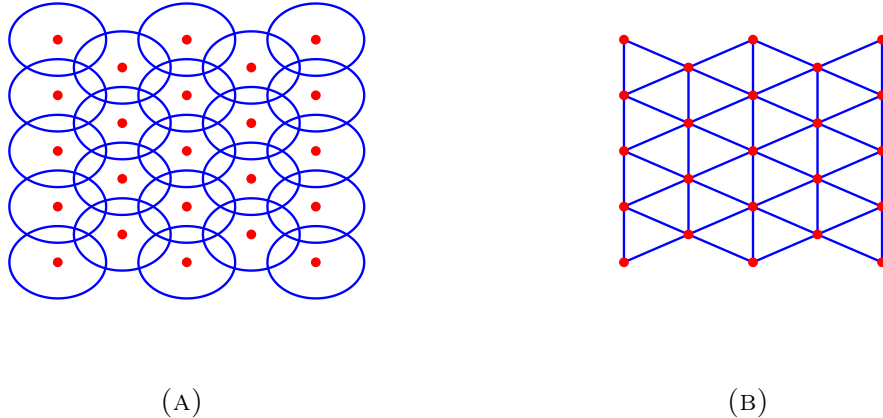


FIGURE 2.1: Schematic of the overlapping sphere model (left) and triangulation model (right). Cell centres are coloured in red. Cell centres that have overlapping circles in the OS model are connected, while cell centres that have edges connecting them in the triangulation model are connected.

Once we have determined the cell connectivity, we need to specify the force interactions between connected cells. Usually, the force between cells is transmitted directly between cell centres in analogy with a standard spring, however more complicated effects, such as torsion, have been implemented in order to produce non-central forces [5]. In the triangulation model, this can be visualised as the forces being transmitted along the edge connecting the two cells.

Usually, there is a term relating to the distance between cell centres. This can include both a repulsive force to prevent cells from getting too close together and an adhesion force to attract nearby cells.

Say we have cells labelled i and j , and their corresponding cell centres labelled \mathbf{r}_i and \mathbf{r}_j , respectively. Assuming an equilibrium separation of the cells s_{ij} , we can define the separation of the cells as $\mathbf{r}_{ij} = \mathbf{r}_i - \mathbf{r}_j$ and the overlap $d_{ij} = s_{ij} - \|\mathbf{r}_{ij}\|$.

The simplest method of describing the force between these cells is a linear spring model, in which the force between cells is proportional to the deviation from equilibrium. Defining k to be the spring constant, we get the force between cells i and j as $F_{ij} = kd_{ij}$.

We can elaborate on this expression by considering cutoffs for when the overlap deviates too far from the equilibrium value. This can be necessary, especially in triangulation based models, for when cells move too far from each other we want for their influence on each other to eventually fade, rather than grow to infinity as the cells are further separated. This can be easily described with the force becoming zero after a certain point, as in [42].

We can also set a hard minimum for the separation between cells, to prevent cells from getting too close to each other. This can be thought of as an infinite potential for sufficiently large overlaps [7]. This can also be represented with more finesse by having the potential grow exponentially after a certain point rather than suddenly having an infinite potential, with the force being linear below a certain overlap and $F_{ij} = kd_{\max} \exp(\kappa(d_{ij}/d_{\max} - 1))$ above some maximum overlap d_{\max} .

For the overlapping spheres models, we can also have some force relating to a function of the area of the two “spheres” of influence that overlap as opposed to the distance between the two cell centres, the simplest example of this being linear repulsive force proportional to the overlapping area [38]. Similarly, we can have an attractive adhesive force based upon overlapping areas, with the shape or radii of the regions of influence for the attractive and adhesive force being in general different.

In order to calculate the movement of the cell centres, we can either use a stochastic method based on potentials or calculate movement based force laws [8]. One common stochastic method is the Metropolis algorithm, as in the cellular Potts model in Section 2.2.1. This may be needed to use for hard-core models with infinite potential wells due to the difficulty dealing with infinite forces.

For calculating the movement directly, the dynamics of the system is usually taken to be overdamped so that inertial movement is ignored, leaving only movement due to forces [7]. Taking the drag coefficient as γ , this gives us the equation of motion

$$\gamma \frac{d\mathbf{r}_i}{dt} = \mathbf{F}_i.$$

In the following, we will base our cell centre model on the linear spring model, using the triangulation method of connectivity and finding the movement of cells based by solving the ODEs produced by the forces. This can be represented in the following equation:

$$\gamma \frac{d\mathbf{r}_i}{dt} = \sum_{j \in N_i} k(||\mathbf{r}_{ij}|| - s_{ij}) \hat{\mathbf{r}}_{ij} + \mathbf{F}_i^{\text{ext}}, \quad (2.1)$$

where \mathbf{r}_i is the location of cell centre i , $\mathbf{r}_{ij} = \mathbf{r}_i - \mathbf{r}_j$, N_i is the set of cells connected to cell i , s_{ij} is the equilibrium distance between the centres of cells i and j , k is the spring constant, γ is the drag coefficient and $\mathbf{F}_i^{\text{ext}}$ is the external force applied to cell i .

There exists a wealth of varying force functions, some of which have been described here, and many of these become increasingly complicated as they further attempt to match observed biological behaviours. However, in bulk systems, these different force functions tend to exhibit similar elastic behaviours, at least in simulations wherein cell connectivity remains constant [32]. There have been some attempts at

including the viscous type of effects seen experimentally. One of these has been in the work of J. Munoz and Santiago Albo [25], where the rest length between cells i and j can change in a manner proportional to the strain of the cells:

$$\frac{\dot{s}_{ij}}{s_{ij}} \propto \frac{||\mathbf{r}_{ij}|| - s_{ij}}{s_{ij}},$$

producing deformation of cell lengths in a manner similar to the Maxwell viscoelastic model. This change in cell lengths is permanent however, on release of the external force, and cell lengths increase infinitely with continued applied stress, making it unsuitable for representing the behaviour of the creep experiment.

2.2.3 Vertex Models

There exist other discrete off lattice models of cell behaviour other than cell centre based models. Another large class of models describe cells as polygons, with these polygons being fully described by the vertices (e.g. Figure 2.2). The choice of polygons as the shape of the cells is motivated by experimental data, with cross sections of epithelial cells showing polygonal structures [17]. These vertex based models usually allow a bit more flexibility in describing systems in comparison to cell centre models due to their higher degrees of freedom [1].

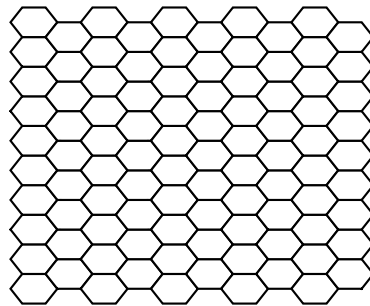


FIGURE 2.2: 10 by 10 grid of hexagonal cells in equilibrium, described by a vertex model. Each cell is connected to its adjacent cells via the sharing of common vertices.

These models have been used, for example, to simulate tissue growth in plants [35] and wound healing [28].

In these cell vertex models, the shape of the cell is explicitly described by the location of its vertices. This is in contrast to the cell centre models seen previously, where the shape of the cell is only implicitly described. The location of the cell can be said to be the set of all points closer to its cell centre than to any other

in such a cell centre model (a Voronoi description of the cell shape), but this isn't an exact description, and a vertex based model gives more descriptive properties of the shape of the cell than the previously described models. Because the vertex description gives a visualisation of cells that is more physically accurate than the cell centre models, often the location of cells in the cell centre models are converted to a Voronoi diagram in order to view the cells as a set of polygons for easier visualisation.

Because the cell vertex models describe the boundaries between cells, they are generally more able to model more complicated inter-cell behaviours than the cell centre models. This includes behaviour such as restructuring the connectivity of a cell monolayer due to internal and external forces shifting the arrangement of cells [11]. This can be done with increased finesse due to the nature of cell connectivity being defined via shared vertices of polygons rather than a binary connectivity status between cells.

One of the most common cell rearrangement actions in vertex models is the *T1 swap* [26]. This T1 swap occurs when two cell vertices get too close together, below some specified minimum separation d_{\min} , where the vertices are moved such that the edge between vertices becomes perpendicular to the old edge between vertices. With this process, cells can retain realistic shapes and allow the cell mesh to restructure.

Similar to the cell centre linear spring model, generally each vertex is assumed to be over-damped, with all movement being due to forces acting upon these cell vertices rather than any inertial components. This can be written explicitly as

$$\gamma_i \frac{d\mathbf{r}_i}{dt} = \mathbf{F}_i,$$

where \mathbf{r}_i is the i th cell with drag coefficient γ_i .

The exact details of these forces depends on the model being used, with there being variety of differing implementations of how these forces are generated.

In Weliky et al. [43, 44], the force on each vertex is the sum of an outward force due to internal cell pressure and tension forces based upon contraction of actin microfilament bundles [30]. The outward force in this model is due to osmotic pressure, and the force is assumed to be directly between the edges connected to this vertex, and is inversely proportional to cell size. The tension forces are modelled as being proportional to the cell circumference and in the direction of neighbouring vertices in the cell. These forces are defined for each cell whose boundary the vertex is a component of, so we sum the forces from each containing cell. The interplay between these two forces then maintain the cell shape and size.

An alternate model follows the developments of T. Nagai and H. Honda [26], where the force consists of a sum of both external forces, and a gradient of a potential. This potential is related to properties of the cells that the vertex belongs to. In

other words, cellular boundaries will be affected both by external forces and the properties of the cells being connected by the boundary [11]. This model, when undergoing constant force, produces an exponential style response consistent with standard viscoelastic materials [18].

The potential to be minimised is a function of all of the cells in the monolayer. Say in our system there are N separate cells, where each cell k is characterised by the set of its vertices. If there are n_k vertices in a cell k , they are each denoted in a 2D plane by the set of tuples $\{(x_{k_j}, y_{k_j})\}_{j=0}^{n_k-1} = \{\mathbf{v}_{k_j}\}_{j=0}^{n_k-1}$.

One of the potentials involved is the deformation energy U_D , which relates to the deviation of cells' area from its natural area (we use the area as opposed to cell volume, as we assume the cells all lie on the same plane and have similar heights in accordance with our setting of a monolayer). Mathematically, this is described by

$$U_D^k = \lambda(A_k - A_{0_k})^2,$$

where λ is a constant describing the magnitude of this deformational energy, A_k is the area of the cell and A_{0_k} is the natural, rest area of the cell k .

Another potential involved is the membrane surface energy, relating to the conservation of the membrane length of cells. This behaves quite similarly to the above deformation energy, and is described as

$$U_S^k = \beta(C_k - C_{0_k})^2,$$

where β is a spring constant, C_k is the circumference of the cell and C_{0_k} is the target circumference of the cell relating to the rest length of the cell membrane.

The final type of potential in this model relates to the intercell adhesion energy. This represents the energy due to the boundaries between cells. This can be described by taking the sum of the energies due all of the boundaries of the cell k , mathematically represented as

$$U_A^k = \sum_{j=0}^{n_k-1} \mu_j^k \|\mathbf{v}_{k_{j+1}} - \mathbf{v}_{k_j}\|,$$

with $(x_{n_k}^k, y_{n_k}^k) = (x_0^k, y_0^k)$. The parameter μ_j^k is dependent on the types of cell on either side of the given cell boundary, and scaled by the length of this boundary.

The sum of all of the given potentials is then used as total potential to determine the behaviour of the cell system:

$$U = U_D + U_S + U_A = \sum_{k=1}^N (U_D^k + U_S^k + U_A^k),$$

$$\begin{aligned} \mathbf{F}_i &= -\nabla_i U + \mathbf{F}_i^{\text{ext}} \\ &= -\nabla_i \sum_{k=1}^N \left(\lambda(A_k - A_{0_k})^2 + \beta(C_k - C_{0_k})^2 + \sum_{j=0}^{n_k-1} \mu_j^k \|\mathbf{v}_{k_{j+1}} - \mathbf{v}_{k_j}\| \right) + \mathbf{F}_i^{\text{ext}}. \end{aligned} \quad (2.2)$$

Computationally, the gradient can be calculated via the use of explicit formulae for cell area and circumference in terms of vertex locations. See Appendix A for details.

2.3 Further Models

There also exist more complicated models, which attempt to include the presence and effects of more cytoskeletal components in the quest for increasing biological accuracy.

One of these models is the finite element formulation [3, 1], where cells are broken up into a finer mesh, usually triangular elements, as in Figure 2.3. Contributions, such as viscous forces from internal cell structures and tensions along the cell edge, from these triangular sub-elements can then be combined and then solved via a finite element method in order to find the force acting on vertices in the system.

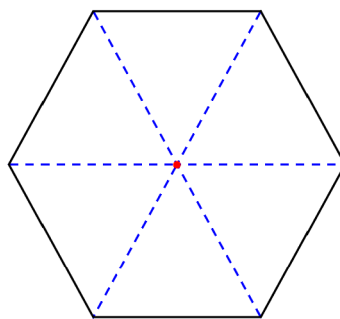


FIGURE 2.3: Example of a hexagonal cell in the finite element model. The cell centre labelled as the red dot, boundaries between triangular sub-elements in dashed blue lines and intercellular boundaries are in black.

Another such formulation is the sub-cellular element model, where cells are described as an ensemble of elements [29]. There exist potentials between these elements within the cell, each of which represents a component of the cytoskeleton such as microfilaments. In this way, a more complete picture of the internal structure of the cell can be produced and modelled in comparison to simpler cell centre or vertex models. When subjected to constant stress forces, these models behave similarly to standard viscoelastic materials, producing exponential creep responses when there is no cell re-arrangement [36].

These models, while being better able to describe more complicated structure and behaviour of the cell, are correspondingly more difficult to implement and more computationally intensive. As available computational power increases over time, it is likely that these types of models will increase in usage as the processing power considerations become less important.

2.4 Summary

In almost all of these models - save for the cell centre attempt to include viscous responses [25] - they are characterised by being dependent on static variables. The system may have been more or less complicated, but mechanical properties are purely dependent on the current state of the system. In order to simulate the different mechanical processes occurring at different rates within the cell in a general way, we want the behaviour of the model to change as we observe the system over longer timescales and their effect becomes apparent.

Chapter 3

Cell Centre Models

In this chapter, we propose a method to represent cellular remodelling for the cell centre linear spring model described previously. Various mechanical experiments will be performed, and the effects of various parameters on the model will be explored. These results will then be compared to the experimental data in Harris et al. [16], and the suitability of the model for the description of empirical phenomena will be discussed.

3.1 Evolving Reference State

To start off, we make some definitions. We define the set of cells that are affected by external forces as the *real state*. This state encodes information about cells that have direct physical meaning; in the cell centre model, the real state is characterised by the set of cell centres. Under this definition, the data modelled under previous cell descriptions would have been in the real state.

To contrast with this, we introduce the *reference state*. Unlike the real state, this state does not have a direct physical meaning; it cannot be affected directly by external forces or be observed to see the outcome of some experiment. Rather, the reference state will encode information to inform the behaviour of the real state. Information from the real state will be able to influence the reference state, and information from the reference state will be able to influence parameters of the real cells. In doing so, the aim is to allow properties of the cells to change over time in response to the application of external forces.

In order to simulate the remodelling, need two sets of variables, the location of ‘real’ cell centres and location of ‘reference’ cell centres. For each cell centre, the location of which is labelled \mathbf{r}_i , we have a corresponding reference cell centre, denoted as ρ_i . In order to for the model to be used, we assume that the reference and real

cell centres have the same connectivity as each other. Define $\mathbf{r}_{ij} = \mathbf{r}_i - \mathbf{r}_j$ and $\boldsymbol{\rho}_{ij} = \boldsymbol{\rho}_i - \boldsymbol{\rho}_j$.

In the simple cell centre linear spring model, we have that forces are modelled as linear springs, with forces in the real state being determined via intercellular distances. We use similar ideas with the addition of the reference state, but the equilibrium spring between two cell centres is no longer static, but rather determined as the distance between the corresponding cells in the reference state. The reference cells on the other hand are modelled as being effected by two different sources. Firstly, between two reference cells there is a linear spring component with equilibrium length equal to the intercellular distance between the corresponding real cells; this allows the reference cells to move and hence modify the parameters of the real state. Secondly, there is a spring force between reference cells with a static equilibrium length, representing the natural length between cells.

In order to incorporate the evolving reference frame into the cell centre model, we modify Equation 2.1 as follows:

$$\gamma_r \frac{d\mathbf{r}_i}{dt} = \sum_{j \in N_i} k(||\mathbf{r}_{ij}|| - ||\boldsymbol{\rho}_{ij}||) \hat{\mathbf{r}}_{ij} + \mathbf{F}_i^{\text{ext}}, \quad (3.1)$$

$$\gamma_\rho \frac{d\boldsymbol{\rho}_i}{dt} = \left(\sum_{j \in N_i} k_S(||\boldsymbol{\rho}_{ij}|| - s_0) \hat{\boldsymbol{\rho}}_{ij} + \sum_{j \in N_i} k_R(||\boldsymbol{\rho}_{ij}|| - ||\mathbf{r}_{ij}||) \hat{\boldsymbol{\rho}}_{ij} \right). \quad (3.2)$$

In this expression, we have the drag coefficient for the reference state γ_ρ , the spring constant referring to the static term k_S and the spring constant referring to the remodelling term k_R . The drag coefficient for the real state has been renamed as γ_r .

First, we non-dimensionalise the equation as follows.

Let $\tilde{r}_i = r_i/s_0$, $\tilde{\rho}_i = \rho_i/s_0$, $\tilde{\mathbf{F}}_i^{\text{ext}} = \mathbf{F}_i^{\text{ext}}/(ks_0)$, and $\tilde{t} = kt/\gamma_r$.

After we substitute, simplify and then drop the tildes for notational simplicity we get the following equations:

$$\frac{d\mathbf{r}_i}{dt} = \sum_{j \in N_i} (||\mathbf{r}_{ij}|| - ||\boldsymbol{\rho}_{ij}||) \hat{\mathbf{r}}_{ij} + \mathbf{F}_i^{\text{ext}}, \quad (3.3)$$

$$\frac{\gamma_\rho}{\gamma_r} \frac{d\boldsymbol{\rho}_i}{dt} = \left(\sum_{j \in N_i} \frac{k_S}{k} (||\boldsymbol{\rho}_{ij}|| - 1) \hat{\boldsymbol{\rho}}_{ij} + \sum_{j \in N_i} \frac{k_R}{k} (||\boldsymbol{\rho}_{ij}|| - ||\mathbf{r}_{ij}||) \hat{\boldsymbol{\rho}}_{ij} \right). \quad (3.4)$$

We then aim to further simplify the equations for the reference state. Let

$$\alpha = \frac{k_S}{k_R + k_S}, \eta = \frac{\gamma_r}{\gamma_\rho} \frac{k_R + k_S}{k}.$$

Making this final set of substitutions we get:

$$\frac{d\mathbf{r}_i}{dt} = \sum_{j \in N_i} (\|\mathbf{r}_{ij}\| - \|\boldsymbol{\rho}_{ij}\|) \hat{\mathbf{r}}_{ij} + \mathbf{F}_i^{\text{ext}}, \quad (3.5)$$

$$\frac{d\boldsymbol{\rho}_i}{dt} = \eta \left(\alpha \sum_{j \in N_i} (\|\boldsymbol{\rho}_{ij}\| - 1) \hat{\boldsymbol{\rho}}_{ij} + (1 - \alpha) \sum_{j \in N_i} (\|\boldsymbol{\rho}_{ij}\| - \|\mathbf{r}_{ij}\|) \hat{\boldsymbol{\rho}}_{ij} \right), \quad (3.6)$$

showing we can completely characterise the behaviour of the model via these two parameters α and η . We define α to be the remodelling ratio, and η the remodelling rate. The parameter α determines the relative strength between the static and remodelling components of the reference state, and η determines the speed of movement of the reference state in comparison to the real state.

All experiments were done on a 10 by 10 hexagonal grid of cells initially at equilibrium (see Figure 3.1). A relatively small grid of cells was chosen to balance realism with computational constraints.

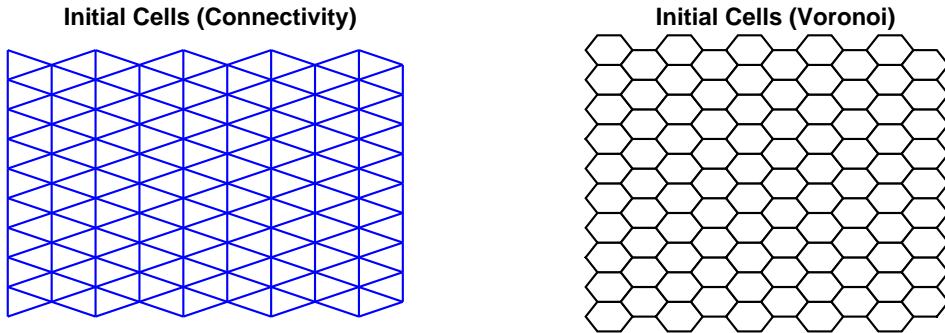


FIGURE 3.1: Initial cell configuration for all experiments is a 10 by 10 hexagonal grid, for both the real and reference cells.

3.2 Creep Response & Stress Relaxation Experiment

In order to assess the properties of this model, *in silico* versions of a creep experiment and a stress relaxation experiment were performed, and results compared to previous models. Full details on the implementation of these experiments can be found in Appendix B, but they are summarised here.

3.2.1 Creep

For the creep experiment, a constant stress was applied to right side of the cells, while the left side was held fixed, recording the strain vs time of the monolayer. The simulation was set to stop if the strain value went above a threshold s_{\max} during the calculation. We chose $s_{\max} = 5$ to avoid overly unrealistic strains. This is above the value that the creep experiment in Harris et al. [16] failed at, but this failure was due to delamination of the monolayer with the testing rods, so a slightly higher value was chosen. An example of the strain as a function of time of such a simulation can be found in Figure 3.2a.

3.2.2 Stress Relaxation

For the stress relaxation experiment, the left side of the cells were held fixed, while the right hand edge was pulled such that the strain of the monolayer increased up to maximum length (set as 1.5 times the original length, due to being in the range of strain values measured in Harris et al.) at a constant rate of strain, and then held at that length. We will call the time it takes for monolayer to be pulled to the maximum strain the *ramptime*. Immediately after the monolayer stops, it was held at the constant strain of 1.5 and we recorded the stress felt at the right edge of the monolayer. The stress-time graph of such an experiment can be found in Figure 3.2b.

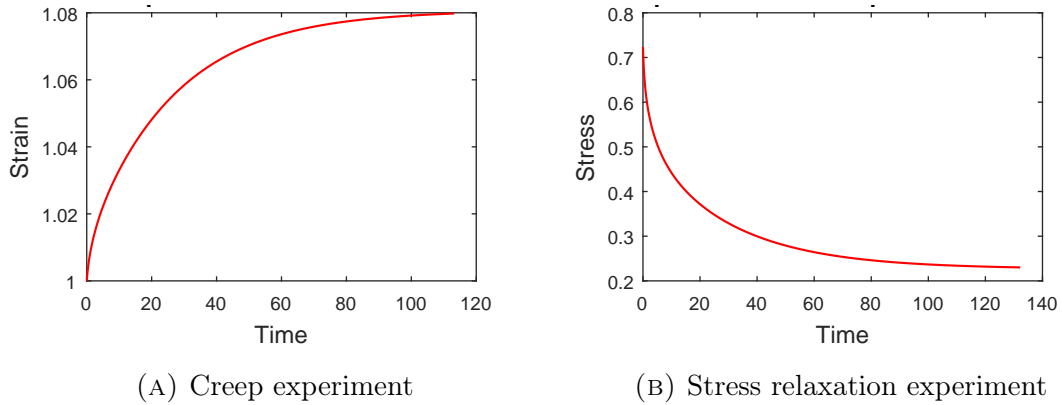


FIGURE 3.2: Example of a strain-time graph for the creep experiment and a stress-time graph for the stress relaxation experiment.

3.3 Multiple Timescales

After looking at the resulting graphs from the creep and stress relaxation experiments, it was observed that there was often two different regions in the graph whereby distinct exponential regions could be distinguished. To capture this behaviour in our simulations we fitted the results with both single and double exponentials (i.e., a sum of exponentials).

Firstly, the y values of all the graphs were rescaled to fit between 0 and 1, so that error comparisons between graphs could be done without bias. In order to display and fit the graphs, an appropriate choice of time interval was necessary, the details of which are described in Appendix D. The data was then fitted with both one exponential and two exponential fits using the inbuilt MATLAB fit function to the equations

$$y_1 = A_1 + B_1 e^{-\frac{t}{\tau_1}}, \quad (3.7)$$

$$y_2 = A_2 + B_{21}e^{-\frac{t}{\tau_{21}}} + B_{22}e^{-\frac{t}{\tau_{22}}}, \quad (3.8)$$

where we choose $\tau_{21} \leq \tau_{22}$ without loss of generality.

We restricted the values of the τ s to be positive in order to capture the effects we were looking for, exponential decay over time as the system reached a steady state. In addition, we required the signs of B_{21} and B_{22} to be the same (negative for the creep experiment and positive for the stress relaxation experiment) so that the calculated exponentials in the two timescale fit corresponded to different aspects of the graph, and not a “lucky” cancellation of a positive and negative exponential.

We further justify the use of sum of exponentials as a method of fitting the data as opposed to stretched exponentials in Appendix C.1.

Examples of the results of such fits, with differing parameters, can be seen in the top half of Figures 3.3 and 3.4, representing examples from the creep and stress relaxation experiments respectively. Note that the two exponential fit in blue will always better than (or equal to) a single exponential fit. We can see the green line (the short timescale component of the two exponential fit) fits the data relatively well for short time, and the yellow line (the long timescale component of the two exponential fit) fits the data relatively well for long time, indicating the two separate timescale realms. We can see on the plot on the right has a greater contribution by the short timescale, and thus can less effectively be represented by a single exponential curve. This can be seen on the bottom half of these figures, where the errors on the right for the creep and stress relaxation examples (Figures 3.3d and 3.4d respectively) have significantly larger errors with a one exponential fit than the figures on the left (Figures 3.3c and 3.4c respectively).

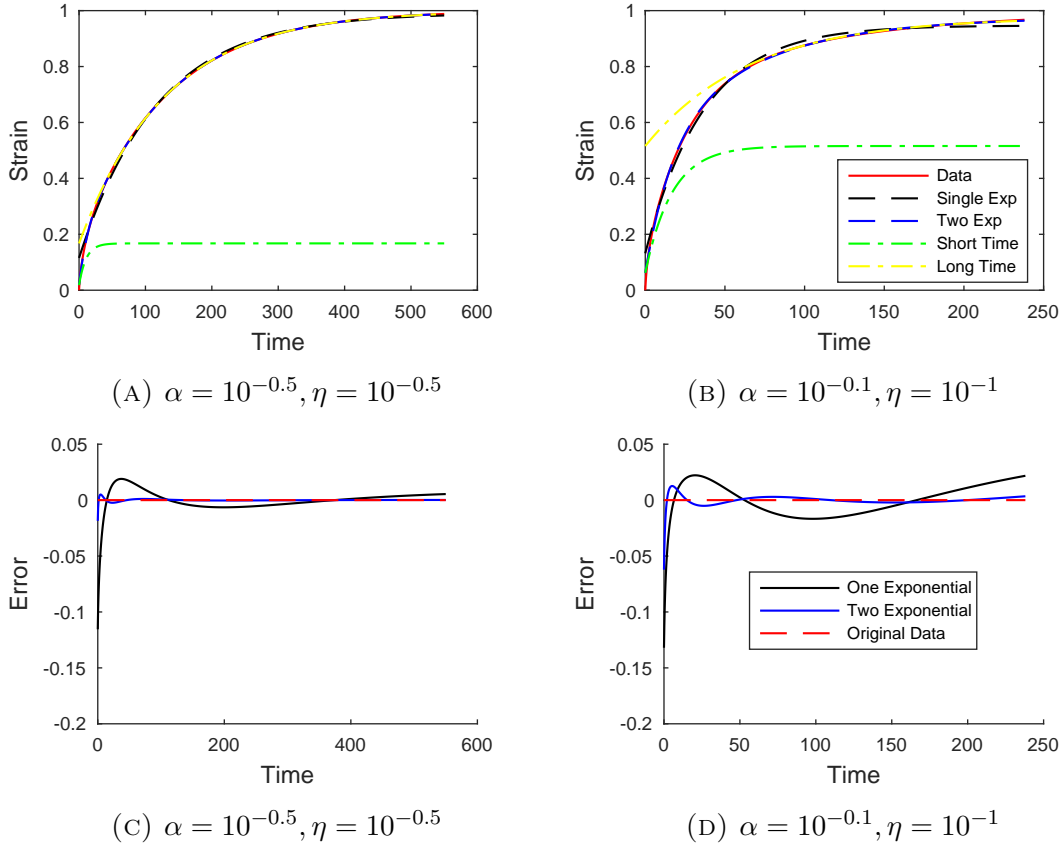


FIGURE 3.3: Top: Examples of a fit of a strain-time curve from the creep experiment. Bottom: Error values for the above plots for each exponential fit. Note the significantly better accuracy for the two exponential fit.

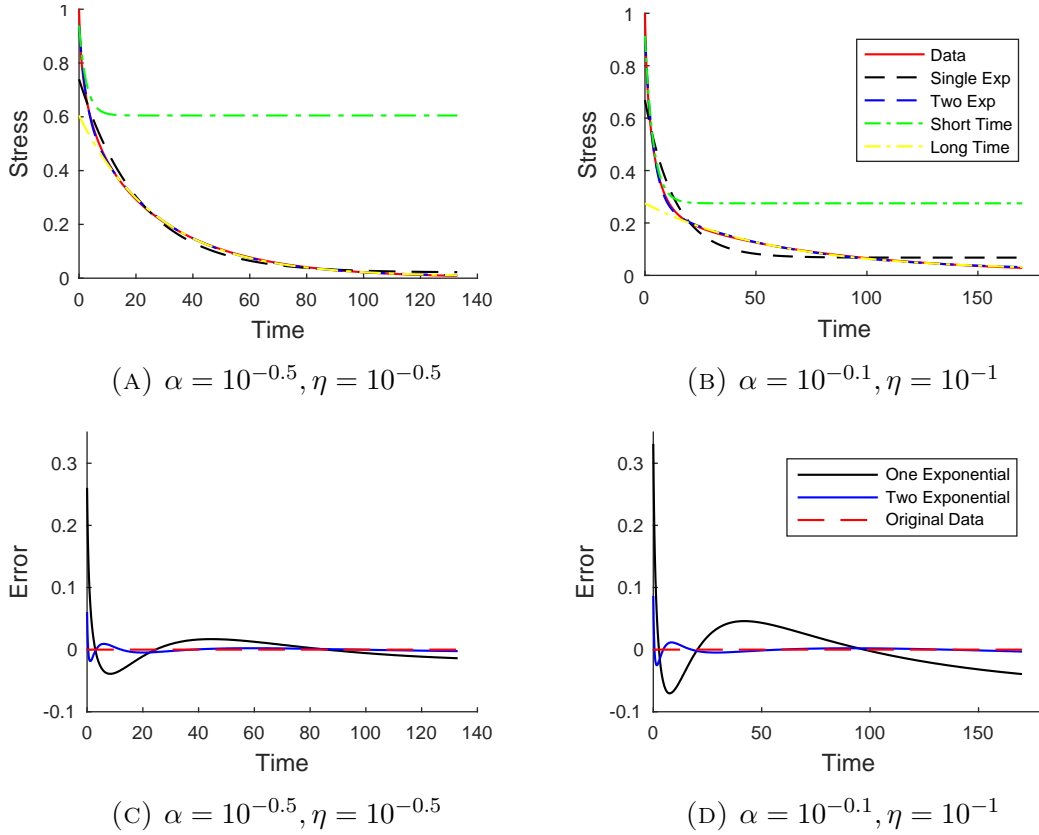


FIGURE 3.4: Top: Examples of a fit of a stress-time curve from the stress relaxation experiment. Bottom: Error values for the above plots for each exponential fit. Note the significantly better accuracy for the two exponential fit.

The idea of using the two exponential fit is that the presence of remodelling should introduce an extra timescale into the problem that can be captured by the second exponential. Having extra parameters in the fit will always increase the accuracy, and therefore we seek a metric to measure the “two-timescaledness” of the problem.

3.3.1 Timescale Metric

When we fit the data with the two exponentials, we get two distinct timescales. The greater the difference between these two timescales, the less well it can be fitted by a single exponential. Therefore, it was decided to use the ratio of two of these timescales, the long double exponential timescale τ_{22} and the timescale of the single exponential τ_1 , as a metric for the two-timescaledness of the data, defining the coefficient ratio:

$$\tau_r = \frac{\tau_{22}}{\tau_1}. \quad (3.9)$$

For example, in 3.4a, we have $\tau_1 = 21.4458$, $\tau_{21} = 2.5485$ and $\tau_{22} = 27.8014$. This gives a coefficient ratio of

$$\frac{\tau_{22}}{\tau_1} = \frac{27.8014}{21.4458} = 1.29.$$

In Figure 3.4b, where the one exponential description is less accurate, we have that $\tau_1 = 13.3991$, $\tau_{21} = 3.7375$ and $\tau_{22} = 58.2138$, giving a coefficient ratio of

$$\frac{\tau_{22}}{\tau_1} = \frac{58.2138}{13.3991} = 4.34.$$

This value of the coefficient ratio is significantly higher than the previous value calculated for the data which can be represented by a single exponential. Some further discussion of this choice of metric can be found in Appendix C.2.

3.3.2 Behaviour of the System Without Remodelling

Before we talk about remodelling, we will first quickly discuss the behaviour of the system without remodelling in more detail. For a single spring, the strain in the creep experiment follows an exponential curve. However, because our system is made up of sets of interconnected springs in a non-trivial manner, we will not necessarily expect to get an exactly exponential response. Tissues are often modelled as viscoelastic materials, which tend to have exponential creep and stress responses to the above experiments, and so we expect a single exponential to be a relatively good fit.

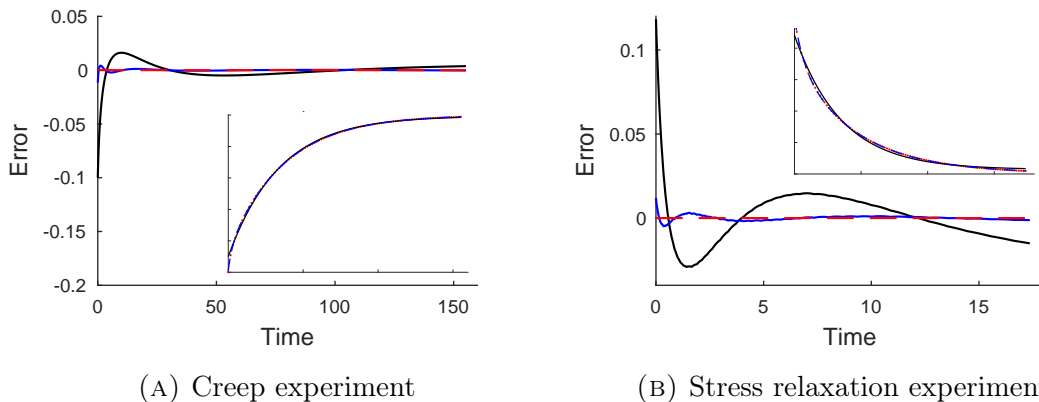


FIGURE 3.5: Differences in one exponential fits (black) and two exponential fits (blue) with no remodelling.

We notice that in the base system, a one exponential fit does not perfectly characterise these curves (Figure 3.5). However, this effect is relatively small, much less than the behaviour seen in Harris et al, and thus the system with no remodelling cannot explain the two timescale phenomena seen.

To look closer at this in the creep experiment, we plot the restoring force, the average of the force opposing the external force on the rightmost cell centres, and the errors of its one and two exponential fits, in Figure 3.6.

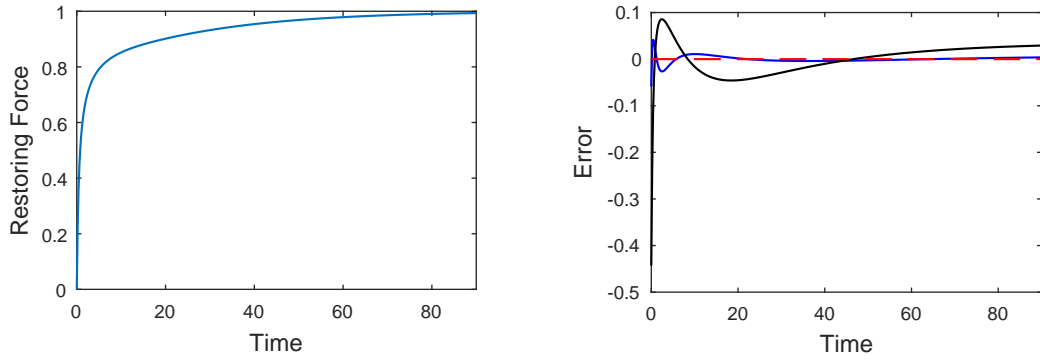


FIGURE 3.6: Left: Restoring force vs time. Right: Restoring force approximation errors, with one exponential in black and two exponential in blue.

We see that the restoring force quickly increases at the start of the experiment as the rightmost cells are pulled, followed by a slow increase as this affects the rest of the monolayer, and that the restoring force itself has two timescales. As the creep is related to the integral of the restoring force, this non-perfectly exponential restoring force causes the creep to not be perfectly characterised by a single exponential.

These effects of non-perfect exponential behaviour due to a discrete model will persist with the addition of the reference state, but will generally be much smaller in magnitude than what will be produced via the reference state.

3.4 The Effect of Remodelling Ratio and Remodelling Rate on Time Scales

To analyse the possible behaviour of our model, the parameters α and η were swept over, and the force applied for the creep experiment, as well as the period of time the strain is ramped up over in the stress relaxation experiment were varied. The values of α and η that were swept over were both between 0.1 and 1, one order of magnitude difference.

3.4.1 Creep Experiment

In Harris et al. [16], increasing the force on the monolayers increased the two exponential behaviour. In the sweep of the creep experiment, in addition to varying α and η , the force values on the right hand side of the cells were varied to see if force variations changed the simulation's multiple timescale behaviour. The force values swept over were 10^{-1} , $10^{-0.5}$, and 10^0 .

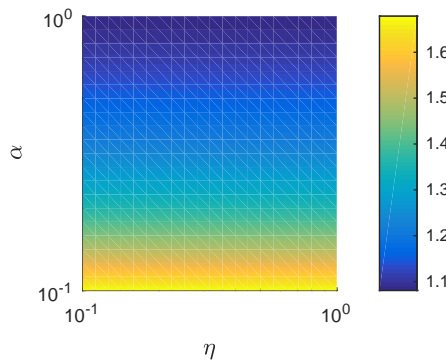


FIGURE 3.7: Final strain of the graphs after equilibrating, subject to a force on the right hand cells of 10^{-1} .

We can see the effect of the remodelling parameters on the final strain of the system equilibrating in Figure 3.7. As we can see, the final strain depends purely on the value of α , the remodelling ratio, and not the remodelling rate η , with higher strain values occurring for lower values of α .

However, the manner in which the monolayer reaches these final strains will depend on both parameters, and so we will analyse this via analysis of their exponential timescales. Some examples of the strain-time graphs and results of exponential fitting to them are found in Figure 3.8.

In Figure 3.8 (a,b), the plots show coefficient and error values for varying parameter values. The blue and black dots represent the long (τ_{22}) and short (τ_{21}) timescales respectively of the fits of the data, while the red dots are the timescale of the one exponential fit (τ_1). The size of the blue and black dots are scaled by the magnitude of the exponential term relating to the timescale. If both exponentials have equal magnitude, both dots will be equally sized at a maximum radius. If one of the exponentials is smaller magnitude than the other, then the smaller exponential will have a correspondingly smaller dot. The red dots relating to the one exponential fit remain at a constant size, the maximum size of the blue or black dots. Notice that the one exponential attempts to compromise between the long and short timescales of the exponential and the timescale lies between the two timescales for the biexponential fit.

In Figure 3.8 (c,d,e), the plots show the errors between the data and the fits of the data, representative of the behaviour of the system in different regions. The error of the one exponential fit is shown in black, while the error of the two exponential fit is shown in blue. The insets show the original data, overlaid with the different exponential fits. The red dots are the original data, the black line is the one exponential fit and the blue line is the two exponential fit.

Figure 3.8f shows τ_r as surface plot, varying over both η and α . The $\alpha = 1$ components of the graph have been removed from the graph, as they are a degenerate case displaying no remodelling.

In Figure 3.8a, we can see that as α decreases, the long timescale (blue) increases in magnitude by a large amount, while the short timescale (black) only increases slightly. This is consistent with the explanation of the reference cells' movement contributing to the long time behaviour of the system, with decreasing α causing the reference state to have greater movement, and thus affecting the long time behaviour of the system. However, at low times, this remodelling doesn't have enough time to take effect, and so the smaller timescale (black) is largely unaffected.

In Figure 3.8b, we can see the effect of varying the remodelling rate η . At high values of η , the long and the one exponential timescales are similar, and get increasingly differentiated as we decrease the remodelling ratio, meaning that the behaviour can be better described as biexponential behaviour for low remodelling rates. This can be understood as at low values of η it takes time for the reference state to be affected by the force changing the distance between cell centres. This allows the real state to initially move at a timescale largely divorced from the effects of the reference state, due to the reference state being effectively static over those periods of time. We then get a long timescale resulting from the movement of the reference state allowing further strain of the real monolayer. However, at large values of η , the two states effectively act in concert, with movement of the real state quickly causing a change in the reference state. This "blurs" the effect of the cellular remodelling and results in largely one timescale behaviour.

We can see an example of this in Figure 3.8c, where there is a large differences in timescales. The data (red) has large variation with the one exponential fit (black), and can be much better approximated a sum of exponentials (blue). This can be seen in the inset strain-time graphs as having a noticeable kink, which is representative of the majority of simulations exhibiting multiple timescales. We will tend to get the greatest presence of biexponential behaviour if effects from the external force acting on the real cells as well as the effects from interactions between the real and reference cells are both of similar magnitude.

Therefore, we get the largest effects at low values of η , when the two regions can clearly be distinguished, and at relatively high values of α , when the initial behaviour not due to the reference state is a non-negligible component. This can be seen in 3.8f as the bright region at the top left corner of the surface plot.

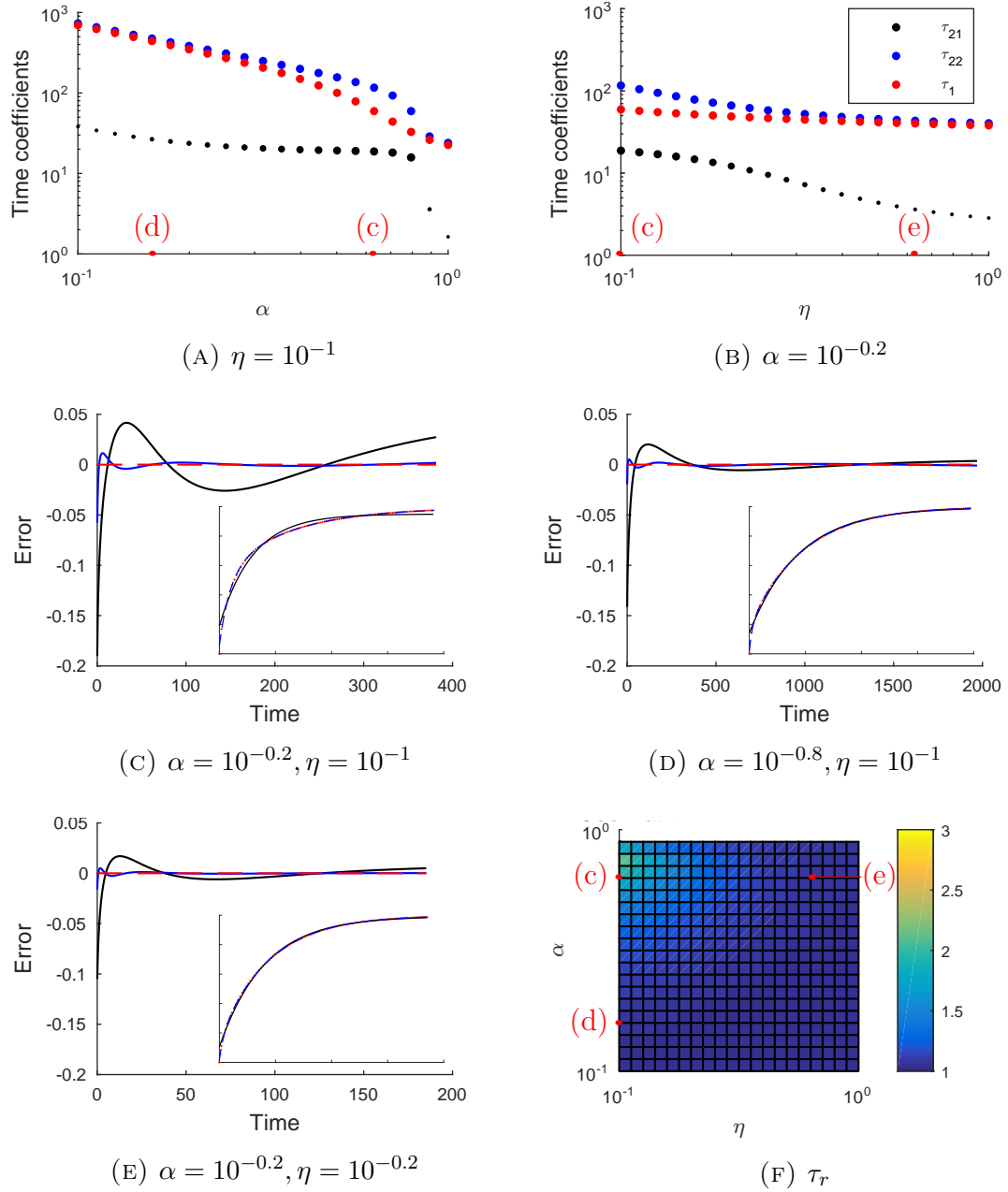


FIGURE 3.8: Example time differences for the creep experiment. All plots were taken with values of force = $10^{-0.5}$.

We can see the small amount of multiple time scale behaviour with no remodelling, by looking at when α equals one. This can be seen in Figure 3.8a in the regions of high α . We can see that timescale of the system with no remodelling (corresponding to α equalling one) is very close to the short timescale of the system as α decreases, further showing that the short timescale corresponds to the system without remodelling. As α approaches one from below, the system transitions from the long timescale representing the remodelling effect to it representing the static effect, and the short timescale transitions from representing the non-remodelling exponential effect to capturing the small amount of multiple timescale behaviour inherent in aggregates of discrete cells.

We can also see the effect of varying external forces on the region of biexponentiality in Figure 3.9. Increasing the force in the creep experiment increases the region wherein the system acts in a biexponential manner (Figure 3.9d, displayed as the enclosed region), as well as the maximum coefficient ratio. This is consistent with the experimental data, where the multiple timescale behaviour in the system becomes more pronounced as the force applied on the monolayer is increased (Figure 1.1).

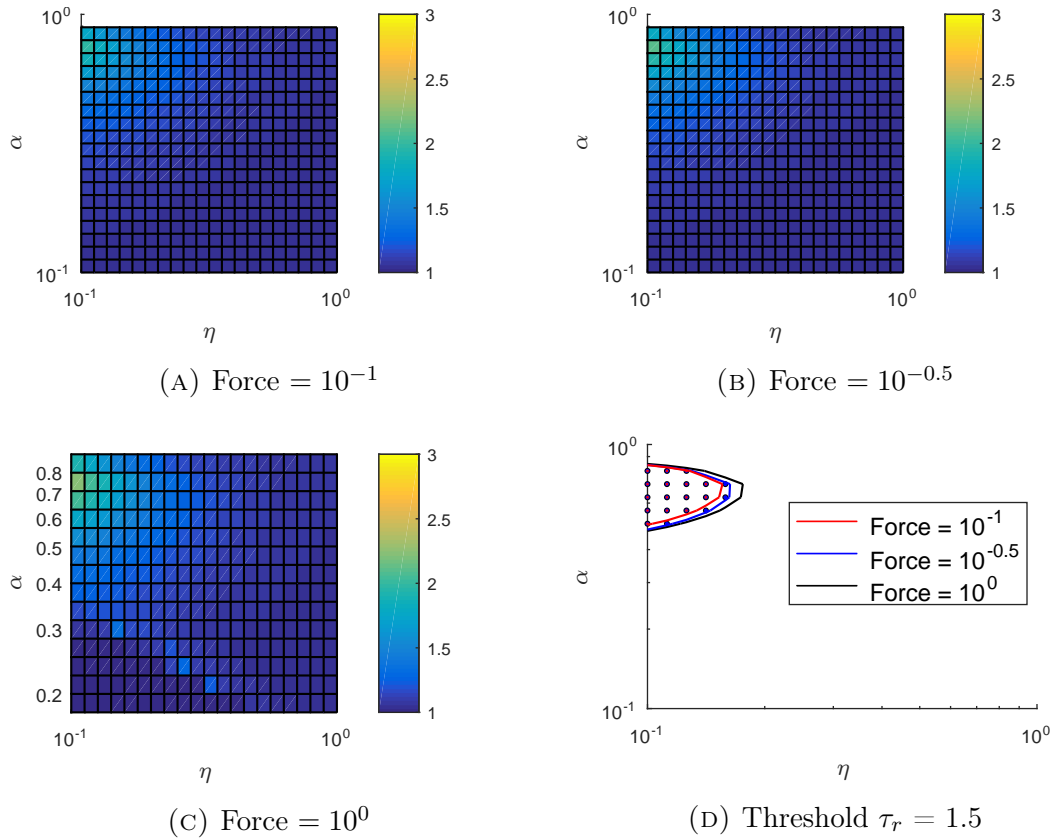
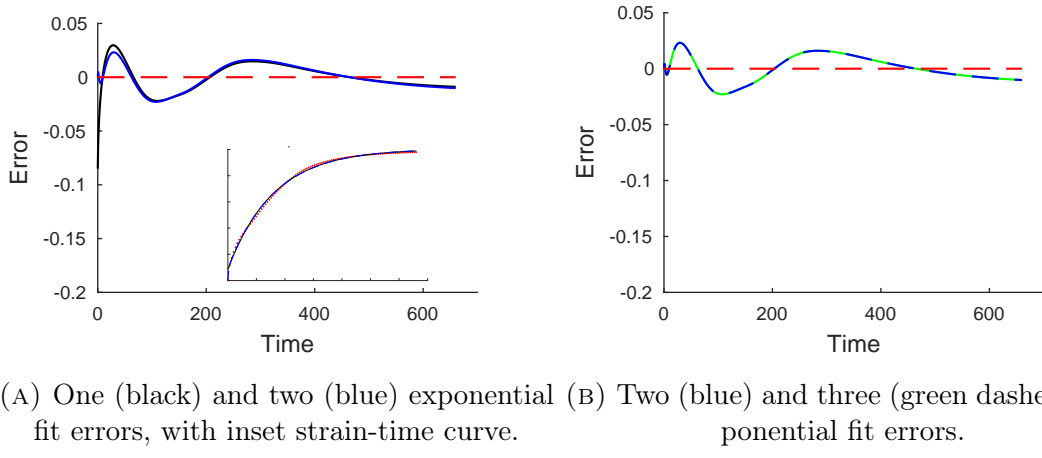


FIGURE 3.9: Surface plots showing varying differences in timescales for different forces in the creep experiment, and compound contour plot showing regions of two exponential behaviour.

Looking at the force = 10^0 surface plot in Figure 3.9c, we see that there is some “noise” in the bottom left hand corner of the plot, where the ratio of coefficients do not act smoothly. If we look at an example of a plot in this region (Figure 3.10a) we see that in such high force regimes, the data cannot be accurately represented by one or two exponentials. Fitting with a higher amount of exponentials (three in the case of Figure 3.10), we don’t see any noticeable improvement, indicating that the data in this region cannot be accurately represented by exponentials. Therefore, the surface plot does not show the same “smooth” behaviour as seen in the other plots, due to the metric of two timescale behaviour no longer being applicable.

In these regions of non-smooth behaviour, the strain values are all above four. In the Harris paper, delamination of the monolayer from the testing rods occurred around a strain value of two, meaning that the simulations with low remodelling ratio and high force are not biologically feasible.



(A) One (black) and two (blue) exponential fit errors, with inset strain-time curve. (B) Two (blue) and three (green dashed) exponential fit errors.

FIGURE 3.10: Example errors of a high force/low α simulation.
 $(\alpha = 10^{-0.6}, \eta = 10^{-1}, \text{Force} = 10^0)$.

3.4.2 Stress Relaxation Experiment

In the stress relaxation experiment, the ramptime values that were simulated over were one order of magnitude, with the values being swept over being 10^1 , $10^{1.5}$ and 10^2 . Some sample stress-time graphs and exponential fits are shown in Figure 3.11.

One of the main differences in the behaviour of the plots between the creep and stress relaxation experiment is the effect of decreasing α . In the creep experiment, decreasing α , and thus increasing the remodelling component, increases the size of the long timescale. However, in the stress relaxation experiment, after an initial increase in timescale due to the addition of remodelling, further decreasing the value of α has little effect (Figure 3.11a). Changing the value of η (Figure 3.11b) has a

similar effect to the creep experiment, with decreasing η decreasing the remodelling speed, causing all the timescales to increase, primarily the long timescale.

With regards to two exponential behaviour, we find similar results to the creep experiment. Regions wherein stress-time curves can be comparatively best fitted by two exponentials are areas of high α values and low η values, where there is the largest distinction between the movements of the real and reference state (e.g., Figure 3.11c), and thus displaying the most multiple timescale behaviour. Simulations further from this region (Figures 3.11d, 3.11e) display significantly less multiple timescale behaviour, as can be seen in Figure 3.11f. In addition, at least for these parameter regimes, stress-time curves from the stress relaxation experiment tend to be less able to be fitted by a single exponential curve. This is evidenced by the greater error values for the one exponential fit in 3.11c, greater contributions of the short timescale compared to the creep experiment (generally larger sizes of the black dots in Figures 3.11a and 3.11b compared to 3.8a and 3.8b) and higher maximum coefficient ratio values in 3.11f.

In Figure 3.12 (a,b,c), we see that decreasing the ramptime, and thus consequentially increasing the strain-rate of loading, increases the maximum magnitude of the coefficient ratio observed. This agrees with the experimental data, with multiple timescale behaviour being more prevalent with higher loading strain-rates (Figure 1.2).

In Figure 3.12d, we can see that as the ramptime decreases (and thus as the speed of the initial ramp increases) we see that the region of biexponential behaviour moves downward, with lower values of α exhibiting multiple time scales. In other words, as the time the strain is ramped over decreases, to compensate for this we need a larger remodelling (lower values of α) component to allow the reference state to sufficiently deviate from equilibrium in the shorter amount of time in order to see multiple timescales.

The change in behaviour as external factors change is a much more dramatic shift for the stress relaxation experiment than the creep experiment, likely due to the inherent external timescale for the stress relaxation experiment (the ramptime), and the lack of an external timescale for the creep experiment. We see that for the creep experiment in Figure 3.9 that a change in force does not really change the shape of the region of multiple timescale behaviour, it simply increases the region that this occurs and the magnitude of the coefficient ratio slightly. However, in the stress relaxation experiment in Figure 3.12, there is a distinct shift in the region of multiple timescale behaviour, and there is a significantly more dramatic increase in the magnitude of multiple timescale behaviour.

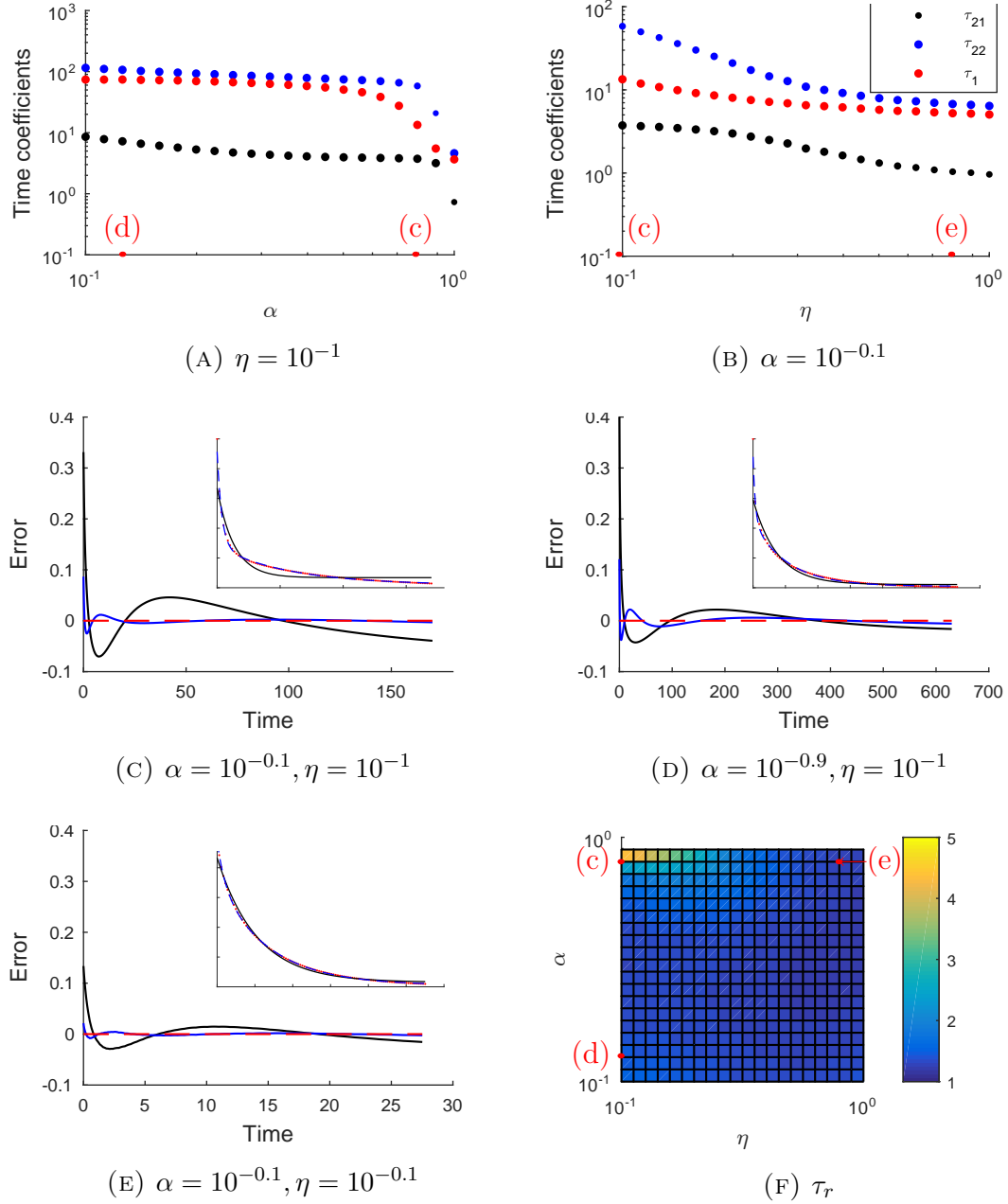


FIGURE 3.11: Example time differences for the stress relaxation experiment, with graphs representing same data as in Fig 3.8. The ramptimes for this experiment were all taken to be $10^{1.5}$. Notice that the forms of the graphs are quite similar to Fig 3.8 , with regions of two exponential behaviour being most prominent around low values of η and high (but not 1) values of α .

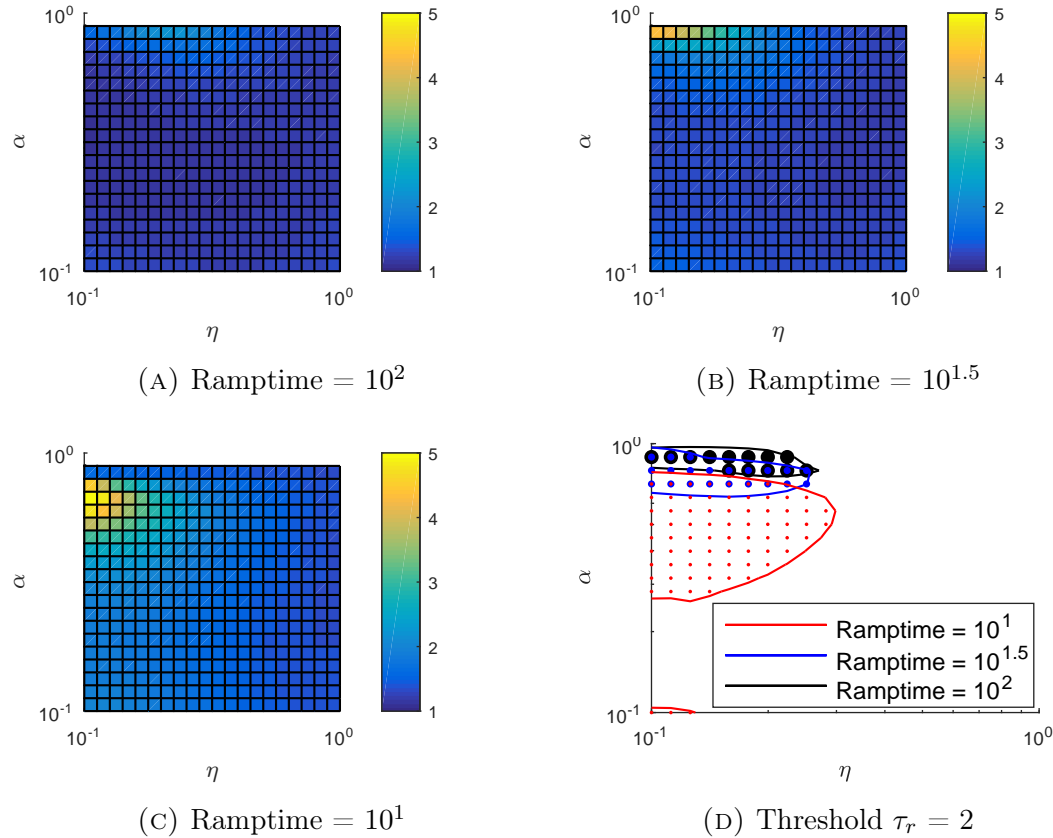


FIGURE 3.12: Surface plots showing varying differences in timescales for different ramp times in the stress relaxation experiment, and compound contour plot showing regions of two exponential behaviour

In Figure 3.12, in the contour plot displaying the 10^1 ramptime, there is a small region of two exponential behaviour in the low η low α region, distinct from the main body of biexponential behaviour. However, the magnitude of the ratio between the two timescales is minimal compared to the low η high α region (differing by a scale of around 2.5). The region is visible due to the increased ratio between the two timescale coefficients from the low ramptime raising this region above the relatively low threshold appropriate for the other ramptime timescale ratios.

3.5 The Addition of Memory Leads to Multiple Time Scales of Remodelling

In order to further investigate the ideas of the time dependency on remodelling, memory was implemented by having the reference state's dynamics depend on a

time average of the real state. This is done by modifying the equations of motion appropriately:

$$\frac{d\mathbf{r}_i}{dt} = \sum_{j \in N_i} (|\mathbf{r}_{ij}| - |\boldsymbol{\rho}_{ij}|) \hat{\mathbf{r}}_{ij} + \mathbf{F}_i^{\text{ext}}, \quad (3.10)$$

$$\frac{d\boldsymbol{\rho}_i}{dt} = \eta \left(\alpha \sum_{j \in N_i} (|\boldsymbol{\rho}_{ij}| - 1) \hat{\boldsymbol{\rho}}_{ij} + (1 - \alpha) \sum_{j \in N_i} k (|\boldsymbol{\rho}_{ij}| - |\bar{\mathbf{r}}_{ij}|) \hat{\boldsymbol{\rho}}_{ij} \right), \quad (3.11)$$

where $\bar{\mathbf{r}}_{ij} = \frac{1}{T} \int_{t-T}^t |\mathbf{r}_{ij}| d\tau$, i.e. it is an average of the previous real lengths, and T is the time to average over. No averaging of the intercellular distances correspond with a value of $T = 0$.

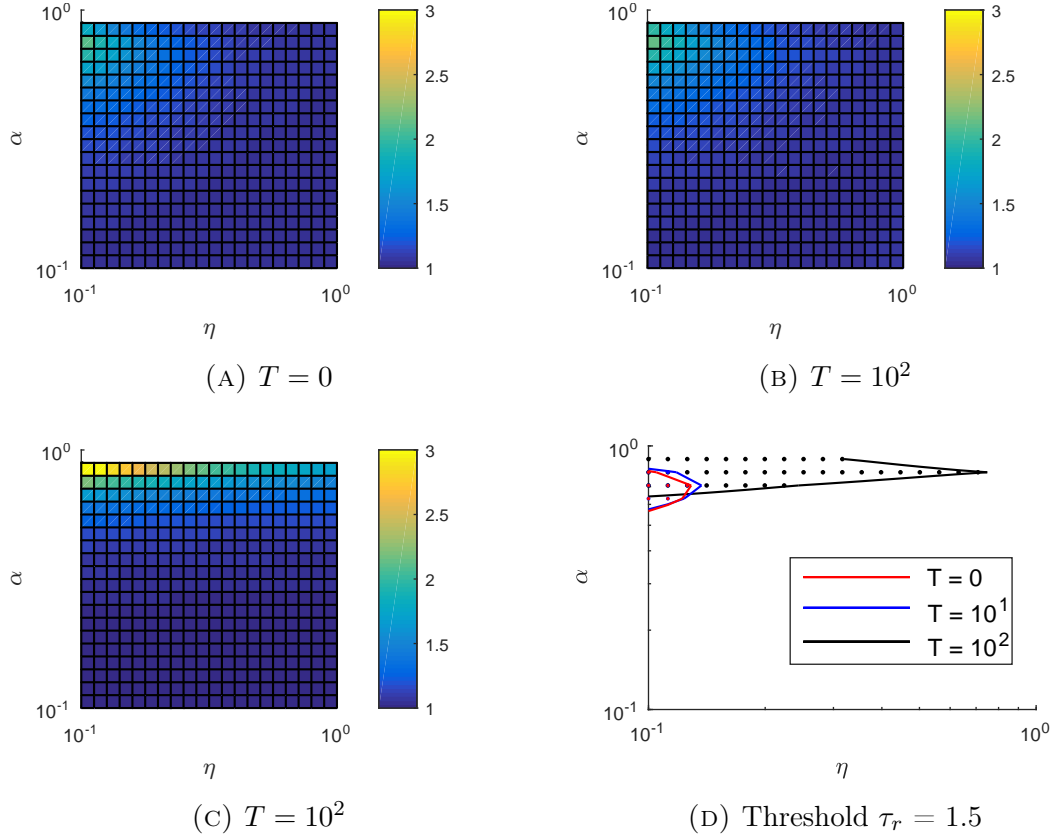


FIGURE 3.13: Surface plots showing varying τ_r values for a sample force in the creep experiment, with differing averaging times. Also included is a compound contour plot showing regions of two exponential behaviour. All experiments were conducted using a force value of $10^{-0.5}$.

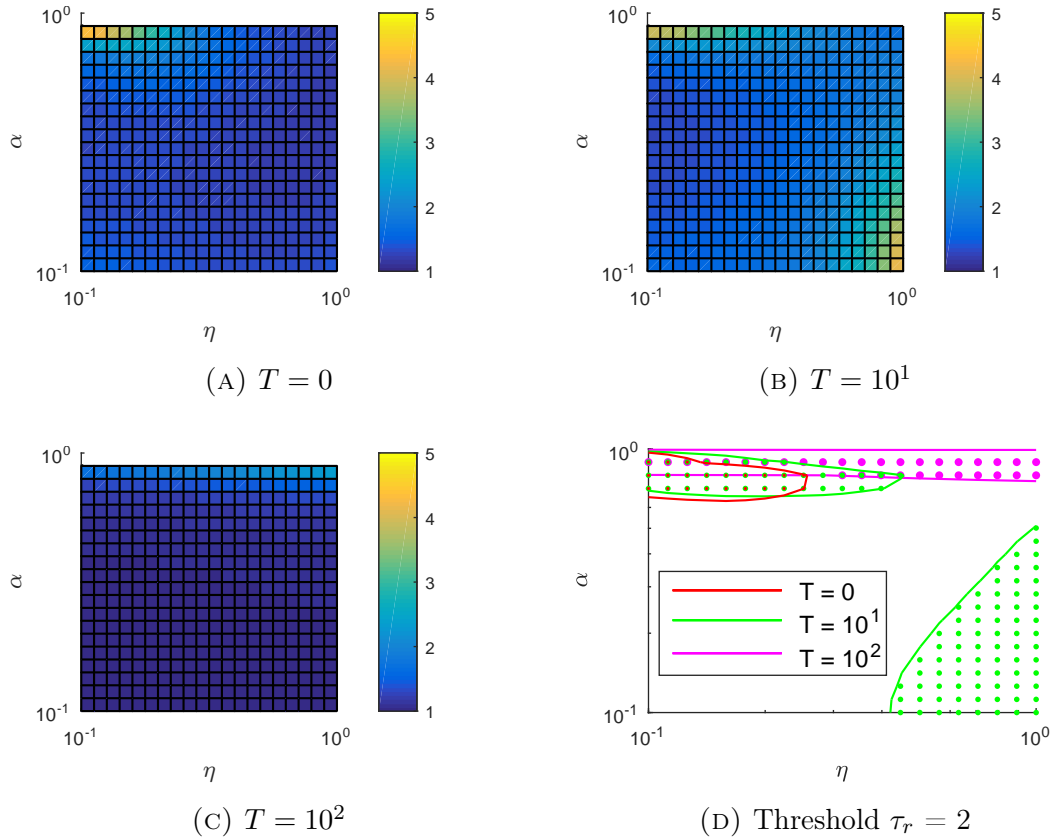


FIGURE 3.14: Surface plots showing varying τ_r values for a sample ramptime in the stress relaxation experiment.

To see the behaviour of the two systems, we plot surface plots and a compound contour plot for both the creep and stress relaxation experiments in Figures 3.13 and 3.14 respectively. From this, we can see the behaviour of the system changing as T is varied.

We can see an example of this in Figure 3.13, where we can see that the largest impact that the addition of memory has is increasing the region of two exponential behaviour along the η direction. This is not too unexpected, as both T and η affect the rate at which information is transferred between the real and reference frames. Therefore, increasing the value of T has the effect of allowing the two regions of behaviour to be clearly distinguished even at higher values of η , and so a larger area of the plot exhibits multiple timescales.

The stress relaxation experiment however exhibits more exotic behaviour than the creep experiment, as we can see in Figure 3.14. Any timescales in the creep experiment come from the model, and therefore interactions between the averaging with

the creep experiment are not that complex. However, in the stress relaxation experiment, there is an additional timescale involved with the presence of the ramptime variable.

At low values of T , we get similar behaviour as the creep experiment, with the upper left region of the plot (values of α close to 1, low values of η) being the primary region of multiple timescale behaviour. However, as T increases, a “lip” at the bottom right hand part of the plot arises (high η , low α) where the presence of delay introduces a new region of biexponential behaviour. However, as the value of T continues to increase, we see that the two timescale regions decrease again, to a similar behaviour as seen in the creep experiment. This suggests that as the averaging time increases, the averaging (vs non-averaging) becomes the dominant effect, and so the system goes back to displaying predominantly one timescale.

We can see examples of this in Figure 3.15. Increasing the value of T initially introduces regions where there are two distinct timescales, but further increases of the averaging time result in curves that cannot be accurately modelled by two or greater exponentials. Therefore, we will get biexponential behaviour from two different sources; one from the high α low η region, being relatively unaffected by the averaging time T and is similar to the creep experiment, and another due to the interaction of the averaging on the system as the strain is applied. This second region is much more complicated due to the multiple competing factors, and is not a two timescale region.

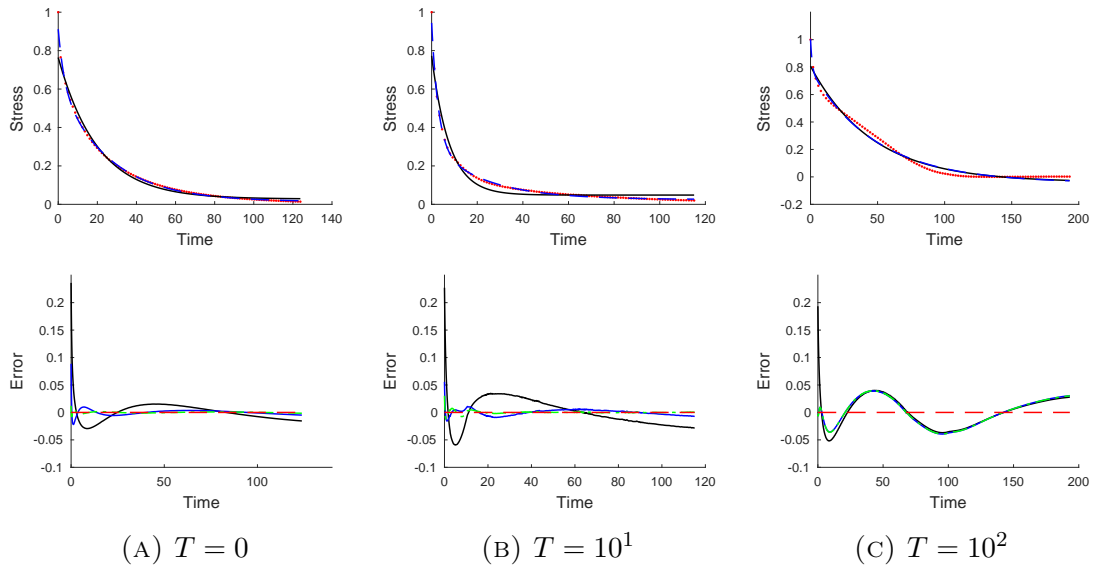


FIGURE 3.15: Top: Example stress-time plots from region of varying biexponentiality as the averaging time T varies. Bottom: Differences in the exponential approximations with the original data, with black being one, blue being two and green being three exponential fits.

Without memory, both the creep and stress relaxation experiment behave similarly with varying η and α , while with the addition of memory there are significant deviations in the two experiments. Coupled with the increased tendency for non-exponential behaviour to be observed, the version of the model without averaging is much more predictable and amenable to analysis.

3.6 Summary

In this chapter, we implemented a reference state in an attempt to represent cellular remodelling, in order to see multiple timescale behaviour as observed in [16]. A parameter sweep over the remodelling parameters, the remodelling ratio α and remodelling rate η , was undertaken over two *in silico* experiments, a creep experiment and a stress relaxation experiment.

Strain and stress curves were then fitted with both one and two exponential fits, and the characteristic timescales of these exponentials were then compared to determine the presence of multiple timescale behaviour.

It was found that the greatest presence of two exponential behaviour, determined by high ratios of timescales for the two fits, was in regions of high remodelling ratio and low remodelling rate, where interactions between the two states were most distinct and separated. Adding in the presence of time delayed averaging increased the areas of biexponential behaviour, but the increased complexity also introduced regions wherein exponential approximations were not appropriate fits.

From this data, we saw the addition of the reference state in these parameter regimes mimicked the effects seen experimentally, with two clear timescales being observed that were not present in the original model. We also found that the extent of this multiple timescale behaviour was more pronounced in response to larger forces and higher loading strain-rates for the creep and stress relaxation experiments respectively, as seen experimentally.

Chapter 4

Vertex Models

Following the representation of cellular remodelling in the cell centre model, we would like implement these remodelling properties in other cell models. Vertex based models are a natural choice of extension, due their ability to react to mechanical forces and their relative ubiquity in tissue simulations. In this chapter, we will attempt to represent cellular remodelling in vertex models, using a reference state as in Chapter 3.

4.1 Implementing the Reference State

Similar to the cell centre model, we introduce a reference state consisting of a set of points with the same connectivity of cells as the real state. Instead of describing the locations as cell centres, the reference state is a set of vertices, with connected vertices describing a set of cells. Each vertex in the real state, \mathbf{r}_i , has a corresponding vertex in the reference state, ρ_i . Vertices describing a common cell in the real state also describe the same cell in the reference state. In other words, as before, the real and reference states describe the same connectivity of the cells, as shown in Figure 4.1.

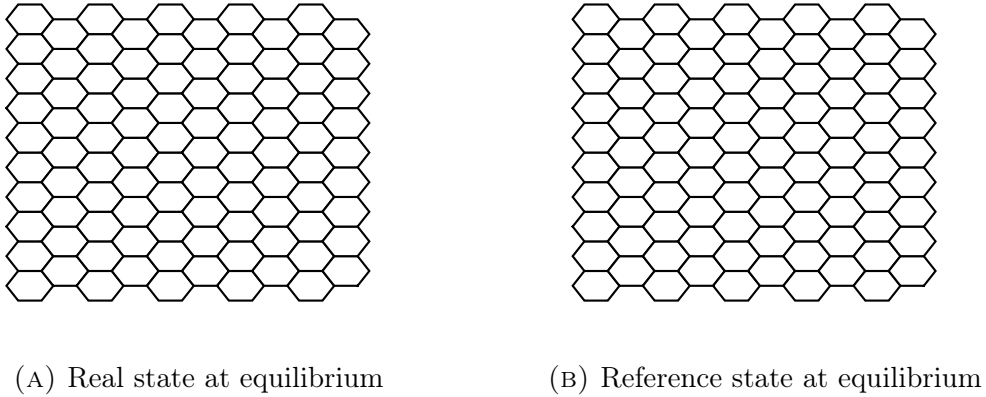


FIGURE 4.1

4.2 Choice of Potential

We would like to describe the evolution of the system with regards to this reference state. For this to happen, we need information from the reference state to inform the evolution of the real state. We also want the locations of the cell vertices in the real state to allow the reference state to evolve.

In the cell vertex model, we will base our model off the work of T. Nagai and H. Honda, as described in Section 2.2.3, where we use the ideas of cell potentials to implement the remodelling. In this formulation, there are three common potentials used, the deformation energy U_D , the membrane surface energy U_S , and the cell-cell adhesion energy U_A .

Both the deformation energy and the cell surface membrane energy have target values in order to minimise the total energy (the cell area and circumference respectively), similar to the intercellular cell length as seen in the linear spring model. However, the cell-cell adhesion energy simply attempts to minimise the length of the cell boundaries.

In accordance with the implementation of the reference state in Chapter 3, we decided to use the cell area and circumference parameters to transfer information between the real and reference states, similar to the intercell distance in the cell centre linear spring. As we were interested in the influence of the reference state on this model, we decided to ignore the cell-cell adhesion energy.

Say we have N different cells and m vertices. Let \mathbf{r}_i be the location of the i th cell vertex and $\boldsymbol{\rho}_i$ be the location of the corresponding reference vertex. We will denote the potential of the real cells as U_r , and the potential of the reference cells as U_ρ . The $2m$ equations of motion describing the system can be written as follows:

$$\gamma_r \frac{d\mathbf{r}_i}{dt} = -\nabla_{\mathbf{r}_i} U_{\mathbf{r}} + \mathbf{F}_i^{\text{ext}}, \text{ for } i = 1, 2, \dots, m,$$

$$\gamma_{\rho} \frac{d\boldsymbol{\rho}_i}{dt} = -\nabla_{\boldsymbol{\rho}_i} U_{\boldsymbol{\rho}}, \text{ for } i = 1, 2, \dots, m,$$

where the coefficients γ_r and γ_{ρ} are the drag coefficients of the real and reference states respectively, and $\mathbf{F}_i^{\text{ext}}$ is the external force.

The real energy is comprised of the deformation energy and the membrane surface energy as detailed above. Let A_k^r be the area of the real cell labelled by k , and A_k^{ρ} be the area of the reference cell labelled by k . Similarly, let C_k^r be the circumference of real cell labelled by k and C_k^{ρ} be the circumference of the reference cell labelled by k . Let A_k^0 and C_k^0 be the natural target area and circumference of the cells respectively. The deformation and the membrane surface energies of a cell k are then described respectively by:

$$U_D^k = \beta(C_k^r - C_k^{\rho})^2,$$

$$U_S^k = \lambda(A_k^r - A_k^{\rho})^2,$$

with β and λ being constants relating to the strength of these respective forces.

In other words, the real energies of a cell are related to the differences between areas and circumferences of the real state and target values obtained from the reference state.

The total energy of the real system is then given by

$$U_{\mathbf{r}} = U_D + U_S = \sum_{k=1}^N (U_D^k + U_S^k).$$

Using the cell centre linear spring model as inspiration, we define a remodelling ratio α and use this to define potential of the reference state,

$$U_{\boldsymbol{\rho}} = \alpha U_{\boldsymbol{\rho}}^0 + (1 - \alpha) U_{\boldsymbol{\rho}}^{\mathbf{r}},$$

where $U_{\boldsymbol{\rho}}^0$ signifies the potential due to static parameters while $U_{\boldsymbol{\rho}}^{\mathbf{r}}$ has potentials dependent on the real cells.

Again, we let the potentials of the reference state be comprised of the sum of the deformation and the membrane surface energy, so that the component of the potential due to static parameters is

$$U_{\rho}^0 = \sum_{k=1}^N \lambda(A_k^{\rho} - A_k^0)^2 + \beta(C_k^{\rho} - C_k^0)^2,$$

and the remodelling component of the potential is

$$U_{\rho}^r = \sum_{k=1}^N \lambda(A_k^{\rho} - A_k^r)^2 + \beta(C_k^{\rho} - C_k^r)^2.$$

Putting all of these components together, we get the equations of motion

$$\begin{aligned} \gamma_r \frac{d\mathbf{r}_i}{dt} &= -\nabla_i \sum_{k=1}^N (\lambda(A_k^r - A_k^{\rho})^2 + \beta(C_k^r - C_k^{\rho})^2) + \mathbf{F}_i^{\text{ext}}, \\ \gamma_{\rho} \frac{d\boldsymbol{\rho}_i}{dt} &= -\nabla_i \sum_{k=1}^N [(1-\alpha)(\lambda(A_k^{\rho} - A_k^r)^2 + \beta(C_k^{\rho} - C_k^r)^2) + \alpha(\lambda(A_k^{\rho} - A_k^0)^2 + \beta(C_k^{\rho} - C_k^0)^2)]. \end{aligned}$$

Finally, we can simplify the system by defining the remodelling ratio η as the ratio of the drag ratios of the two states:

$$\eta = \frac{\gamma_r}{\gamma_{\rho}},$$

to give the final equations of motion (rescaling t as t/γ_r):

$$\frac{d\mathbf{r}_i}{dt} = -\nabla_i \sum_{k=1}^N (\lambda(A_k^r - A_k^{\rho})^2 + \beta(C_k^r - C_k^{\rho})^2) + \mathbf{F}_i^{\text{ext}}, \quad (4.1)$$

$$\frac{d\boldsymbol{\rho}_i}{dt} = \eta \left(-\nabla_i \sum_{k=1}^N [(1-\alpha)(\lambda(A_k^{\rho} - A_k^r)^2 + \beta(C_k^{\rho} - C_k^r)^2) + \alpha(\lambda(A_k^{\rho} - A_k^0)^2 + \beta(C_k^{\rho} - C_k^0)^2)] \right). \quad (4.2)$$

Due to the increased complexity of the vertex model in comparison with the cell centre linear spring model used in the previous chapter, there is a range of parameters that need to be chosen for use in this model. Parameters such as λ and β were chosen based on experimental parameters in previous work, such as in [27].

In all of the experiments done, the initial monolayers for both the real and reference state were a set of regular hexagonal cells. The parameters A_k^0 and C_k^0 were both chosen in accordance with this, so that in the absence of any external forces, the cells are at equilibrium. Therefore, the cells were chosen to have some constant target area $A^0 = A_k^0$ for all values of k , equal to the initial area of the cells (which was

chosen to be 1). Similarly, a constant target perimeter $C^0 = C_k^0$ was chosen as the initial circumference of the cells (which was $\sqrt{8\sqrt{3}}$). Finally, in order to make sure the system behaves as expected, the simulation is set to stop if the self-intersection of cells is encountered.

4.3 Creep Experiment - Testing Setup

Having established the equations of motion, we can run experiments using the vertex model. The experiment in essence is the same as for the cell centre model creep experiment, but some slight modifications need to be made to the testing setup to account for the differences between the models.

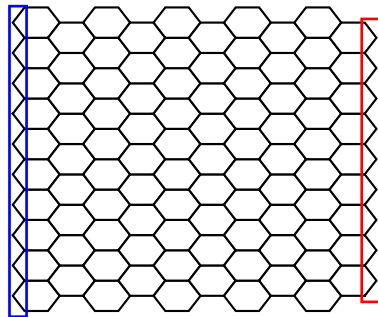


FIGURE 4.2: Vertices on the left in the blue box are held fixed, while the vertices on the right in the red box are moved with constant force.

As can be seen in Figure 4.2, the vertices in the first two ‘layers’ of the cell horizontally are the ones that are subjected to external forces, either being held in a constant position on the left hand side of the monolayer, or being pulled to the right with constant force. As in the creep experiment for the cell centre model (Appendix B), the relative locations of the vertices being subjected to external forces are fixed in order to keep in line with the testing apparatus in Harris et al., with vertical forces being ignored and horizontal forces on the vertices being moved averaged over the vertices in question.

The reason why the first two layers of vertices are the ones held fixed is due to them being the vertices that will be connected to the next layer of cells horizontally. As in the creep experiment in the cell centre model, we want the first layer of cells to be held fixed, connected to the testing rods, and thus held in constant relative position. These are the cells that will be connected to the vertices enclosed in the rectangles in Figure 4.2. This is essentially the same as having an extra layer of cells on both the left and right of the monolayer and holding these completely fixed relative to each other, but this adds extra computational overhead for no gain.

If this is not done, and the creep experiment is performed pulling the rightmost side of vertices only, we get a large increase in strain initially as these vertices are pulled to the right, initially not affecting the area and circumferences of the cells significantly. This means that in the strain-time graphs we see an initial kink as the rightmost vertices are pulled, until the following set of vertices “catch up” and the behaviour of the system becomes representative of the rest of the experiment.

4.4 Interaction Between States in Creep Experiment

In doing the creep experiment with this model, we notice several unwanted effects not observed when applying the reference state to the cell centre linear spring model.

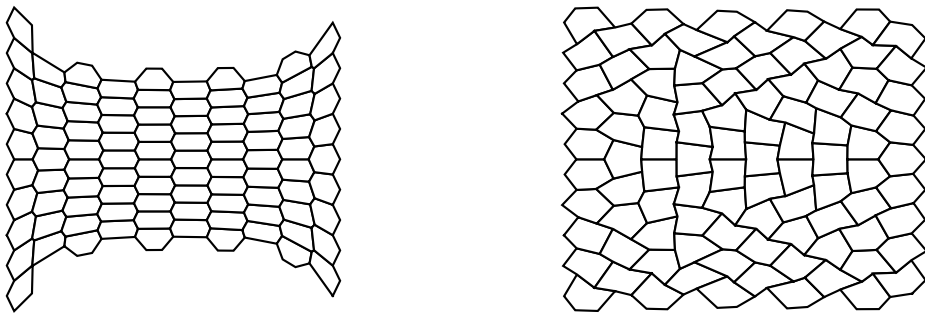


FIGURE 4.3: Resulting real (left) and reference (right) states after the creep experiment, using the parameters $\alpha = 0.2$, $\eta = 1$, $\lambda = 100$, $\beta = 10$.

We can see the results of one such creep experiment in Figure 4.3. The resulting real state appears to be consistent with expectations, with the general structure appearing to be a set of stretched and slightly deformed regular hexagons due to the force applied to the monolayer, with the cells being clearly convex. This is significantly different from the form seen in the reference state. In the reference state, there are many cells which have become concave. This is a problem, as concave cells in this model can potentially ‘buckle’ and even lead to self-intersection of cells.

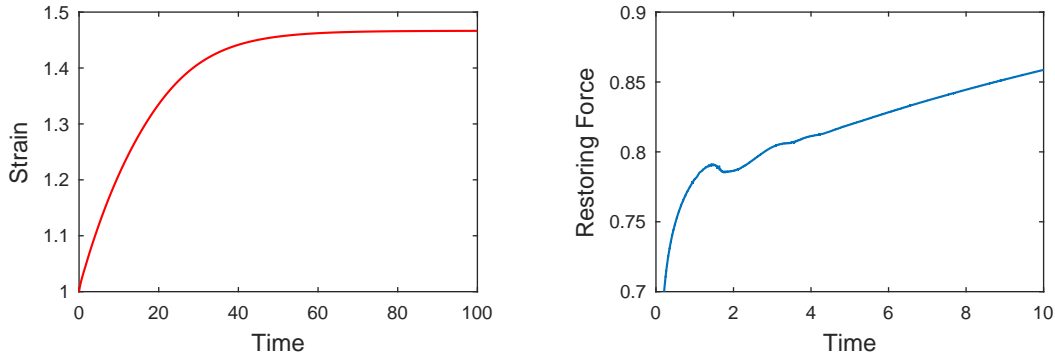


FIGURE 4.4: Strain (left) and restoring force (right) graphs for same experiment as Figure 4.3. The restoring force's non-monotonic feature is zoomed into.

We can also observe other unwanted side effects in Figure 4.4, where the restoring force of the vertices being pulled to the right in the creep experiment are plotted, along with the strain. Notice that the restoring force is non-monotonic - the monolayer puts up less resistance as time progresses as the reference state relaxes to a more energetically favourable state in response to the changing parameters of the system. The restoring force experimentally and in the cell centre linear spring model was monotonically increasing (evidenced by a constantly decreasing derivative of strain vs time leading to exponential curves).

These affects are due to the interactions between the target area and circumference in the reference state shifting in accordance the changing cell shape in the real states. As these target values shift away from the target values for a regular hexagonal grid, the cells change shape accordingly, producing the effects seen above. These shapes vary considerably depending on the force applied via the creep experiment and the parameters used in the simulation, to match whichever configuration is most energetically favourable, and generally do not appear to be predictable. This complicates the situation considerably and makes analysing the behaviour of the system quite difficult.

4.5 Synchronising Area and Circumference

Due to the unwanted effects above, a first attempt to fix this was to force the reference state's cells to behave close to a hexagonal grid. This can be done by synchronising the values of the target circumference and area in the reference state in order to ensure that the cells in the reference state are close to regular hexagons.

We attempted to do this by taking the circumference from the real state and calculating an implied area resulting from this, and using this for the remodelling

component of the time evolution of the reference state. We also attempted the converse of this, with calculating an implied circumference from the area. These two possibilities can be mathematically represented as

$$\frac{d\boldsymbol{\rho}_i^A}{dt} = \eta \left(-\nabla_i \sum_{k=1}^N \left[(1-\alpha)(\lambda(A_k^\rho - A_k^r)^2 + \beta(C_k^\rho - C_k^{A(r)})^2) + \alpha(\lambda(A_k^\rho - A_k^0)^2 + \beta(C_k^\rho - C_k^0)^2) \right] \right), \quad (4.3)$$

$$\frac{d\boldsymbol{\rho}_i^C}{dt} = \eta \left(-\nabla_i \sum_{k=1}^N \left[(1-\alpha)(\lambda(A_k^\rho - A_k^{C(r)})^2 + \beta(C_k^\rho - C_k^r)^2) + \alpha(\lambda(A_k^\rho - A_k^0)^2 + \beta(C_k^\rho - C_k^0)^2) \right] \right), \quad (4.4)$$

where

$$A_k^{C(r)} = \frac{\sqrt{3}}{24}(C_k^r)^2, \quad C_k^{A(r)} = \sqrt{8\sqrt{3}A_k^r}.$$

These final two definitions result from the geometry of a regular hexagon. Equation 4.3 has a reference state which tracks area and calculates an implicit circumference and Equation 4.4 tracks circumference and calculates an implicit area.

We can see that when using this model for the creep experiment the reference state, as expected, looks primarily like a set of regular hexagons (Figure 4.5b). In addition, the restoring force on the right hand side of the cells is monotonically increasing as expected (Figure 4.6).

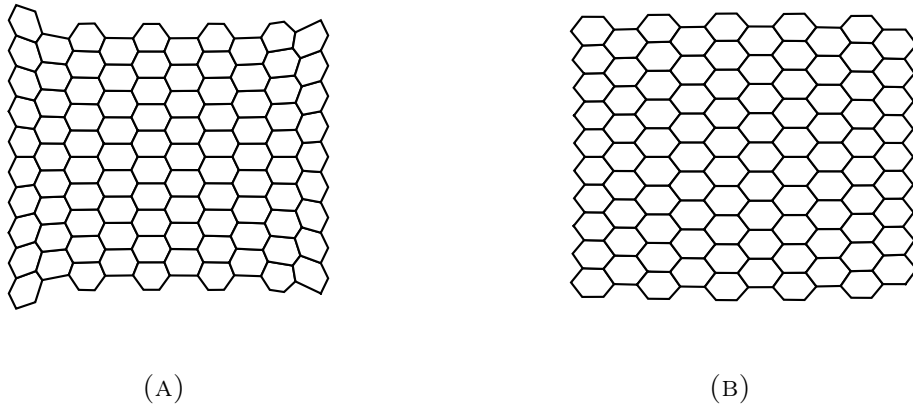


FIGURE 4.5: Resulting real (left) and reference (right) states after creep experiment, using the parameters $\alpha = 0.4, \eta = 1, \lambda = 100, \beta = 10$, with target area in the reference state being calculated from target circumference.

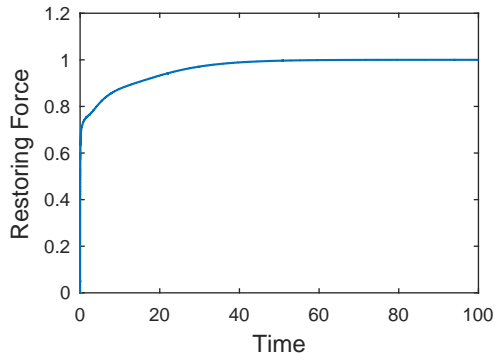


FIGURE 4.6: Restoring force vs time for the same experiment as Figure 4.5.

However, when using this model, we can get feedback loops between the two states. If an implicit target circumference is calculated from the target area, these feedback loops can cause the cell size to approach 0. A similar thing can happen if an implicit target area is calculated from the target circumference, but the feedback loop can cause a runaway increase in cell size, which can then lead to cell self intersection and thus cessation of the simulation. Both of these occurrences cause numerical singularities and breakdown of the simulation. Examples of these can be seen in two creep experiments with the same parameters except for differing in whether the area or circumference is being tracked, in Figures 4.7 and 4.8. Figure 4.7 displays a simulation with circumferences being calculated from areas as in Equation 4.3, where the cell size shrinks and the simulation halts due to a shrinking timestep needed to match the solver's tolerance. Figure 4.8 shows a simulation with areas being

calculated from circumferences a la Equation 4.4, where the cells on the rightmost layer of the monolayer massively expand, ultimately causing the second layer of cells from the right of the monolayer to self-intersect.

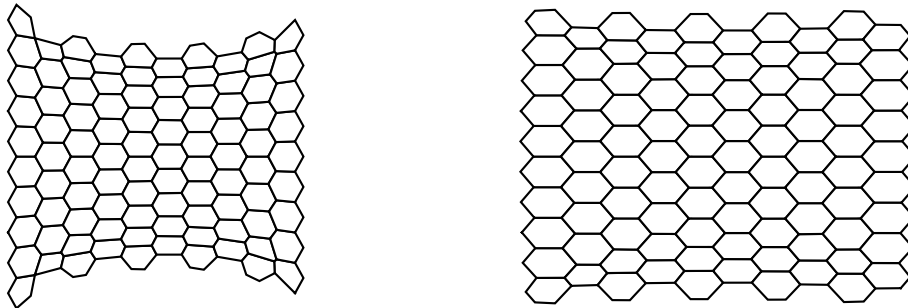


FIGURE 4.7: Real (left) and reference (right) states immediately before MATLAB's `ode15s` halts, when tracking the area and calculating a circumference. Creep experiment, with $\alpha = 0.2$, $\eta = 1$.

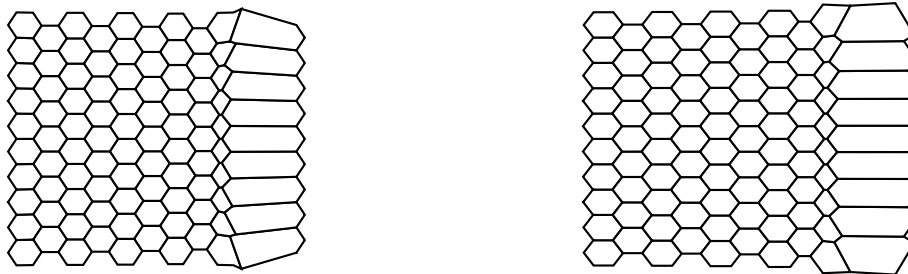


FIGURE 4.8: Real (left) and reference (right) states immediately after self intersection, when tracking the circumference and calculating an area. Creep experiment, with $\alpha = 0.2$, $\eta = 1$.

In the original formulation of the reference state in the vertex model in Section 4.4, area and circumference were separately tied to both the corresponding value in the other state and a static value, preventing too large of a deviation from the target circumference and area values. However, by attempting to synchronise area and circumference we end up ignoring one of these values, resulting in situations where significant enough deviations from the hexagonal equilibrium state can cause the implied area or circumference to be significantly different to the actual values. This can then allow the effect of the remodelling component in the reference state to overpower the static component, causing an increase or decrease of cell size in the real state, which then affects the reference state again and causes a feedback loop.

These singularities are more likely to occur at low values of α , in other words when there is a greater cellular remodelling component. However, they can occur for any value of α less than one if the simulation encounters a sufficiently non-regular shape.

Various averages were attempted to be taken of the target area and the circumference for use as common target cell sizes in the reference state, but these only slightly ameliorated the problem, with numerical singularities still tending to occur for certain parameter values.

4.6 Cell Directionality

In order to implement the cellular remodelling effects, we want to have a component that preserves the shape and structure of the cells in the monolayer with respect to some static configuration, and a component that tracks the movement of cells as they are moved. In the above models, we have used the area and circumference to track both of these effects.

However, we have seen from above that this latter remodelling component does not behave well when tracking area and circumference. Therefore, we want some other component to measure the remodelling of the cell. To do this, we compare our remodelling in the vertex model with the cell centre linear spring model and note that currently, the remodelling component is isotropic; the circumference and area of a cell may change, but the resulting effects from these changes are applied to all vertices present in the cell and not in the direction of change.

In the cell centre models, all of the distances that are measured and recorded are the distances between cell centres. These distances between cell centres are used to calculate forces in the direction between those two cells, and thus these intercellular distances have an inherent directionality encoded within them. Looking at Figure 4.3 and Figure 4.5's remodelling components, we notice that there is no indication of the horizontal stretching of the real state. Either we see that reference cells appear to be deformed in Figure 4.3 or we see a uniform increase in size as in Figure 4.5.

Therefore, for our reference state we want a component which can track the change in monolayer structure taking direction into account.

We will first attempt to implement this idea without a reference state, before adding this effect with the idea of a reference state. The first idea to calculate these effects included the ideas of using the principal axis of the cell; in general, the principal axis of a polygon can be found, and the length and direction of the principal axis vector could be used as parameters in a cell model to include directional ideas. However, in using these values as potential parameters, finding the gradient of these values with respect to vertex locations is required to produce equations of motion to be used in implementing this numerically. Unfortunately, when used upon shapes with

multiple axes of symmetry (such as hexagons) this results in numerical singularities, and is thus an inappropriate model to use.

In lieu of this, we used a similar idea to what is used in a cell centre model; having a springlike component between the two furthest vertices in each cell. This should give an implicit directional component in the model, similar to the effects seen in the cell centre model. This is represented mathematically as

$$\mathbf{F}_i = -\nabla_i \sum_{k=1}^N (\lambda(A_k - A_{0k})^2 + \beta(C_k - C_{0k})^2 + \delta(L_k - L_{0k})^2) + \mathbf{F}_i^{\text{ext}}, \quad (4.5)$$

where L_k is the maximum distance between any two vertices, L_{0k} is the target length of the cell, and δ is the spring constant.

Physically, this new component represents the tendency for the cell to reshape preferentially along its principal axis, due to the anisotropic nature of the cytoskeleton within the cell. Higher values of L_{0k} would cause the cell to preferentially aim for a longer shape, compared to a circular shape.

Some examples of this addition are shown in Figure 4.9, where the creep experiment was performed for a range of values of δ , with simulations having a uniform target length $L_{0k} = L_0$. The force was chosen such that the strain with no length targeting component in the model was found to be 1.1.

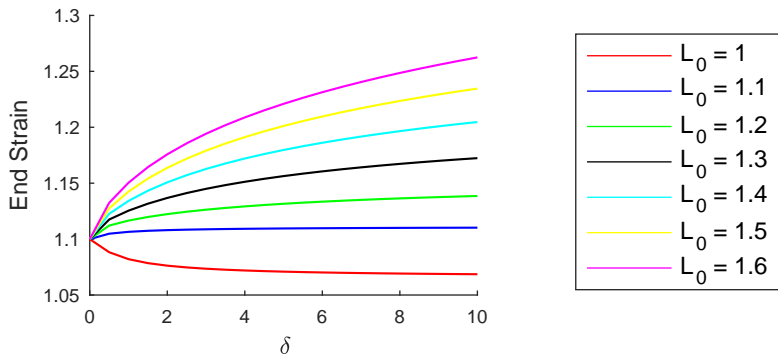


FIGURE 4.9: Final strain for varying values of δ for differing target lengths, where the equilibrium length of a cell was scaled to be equal to 1. $\lambda = 100$, $\beta = 10$, $\mu = 0$.

We can see that as we increase the target length, the final strain increases in the creep experiment. Parameters were chosen so that the final strain was 1.1 with $\delta = 0$, i.e., without the length term. We notice that for target lengths at or above this value, increasing the value of δ increases the contribution for this component of force and thus increases the total strain. Similarly, for the target length below the

final strain (the red line with target length of 1 cell length), increasing δ inhibits the stretching of the cells and decreases the final strain.

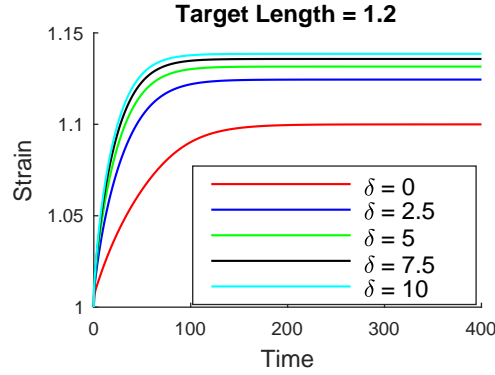


FIGURE 4.10: Strain-time graphs for given target length, varying δ .

Increasing δ both increases the final end strain as well as decreasing the time it takes to reach equilibrium (Figure 4.10). Notice from both of these graphs that the increase in strain from increasing δ plateaus after a while, without reaching the strain value corresponding to the increase in cell length. This can be understood as the cells' major axis not being perfectly in line with the horizontal, the direction where the creep is applied and the strain is measured from, as stretching the monolayer tends to cause the middle of the monolayer to thin and thus change the orientation of the cells.

4.7 Directionality with Reference State

We can now look at implementing this length term with the coupled reference state. As we are attempting to represent the remodelling process through this axial direction through the cell, the form of the remodelling will include a static component of the reference state corresponding to target circumference and area, as well as a remodelling component corresponding with the axial component illustrated in the above section. Again, we ignore the cell interface energies μ for simplicity. This can be represented mathematically as:

$$\frac{d\mathbf{r}_i}{dt} = -\nabla_i \sum_{k=1}^N (\lambda(A_k^r - A_k^0)^2 + \beta(C_k^r - C_k^0)^2 + \delta(L_k^r - L_k^\rho)^2) + \mathbf{F}_i^{\text{ext}}, \quad (4.6)$$

$$\frac{d\boldsymbol{\rho}_i}{dt} = \eta \left(-\nabla_i \sum_{k=1}^N [(1-\alpha)(\lambda(A_k^\rho - A_k^0)^2 + \beta(C_k^\rho - C_k^0)^2) + \alpha\delta(L_k^\rho - L_k^r)^2] \right). \quad (4.7)$$

Unlike in the previous models, due to the static and remodelling components of the reference state representing different forces and changing differing target parameters, having a remodelling ratio of zero does not lead to an infinite strain in the creep experiment. The static component tracking area and circumference will always be present, increasing in strength as the system moves further from equilibrium. In our implementation of this model, we set the static values of area and circumference as has been done previously, having target areas and circumferences of regular hexagons.

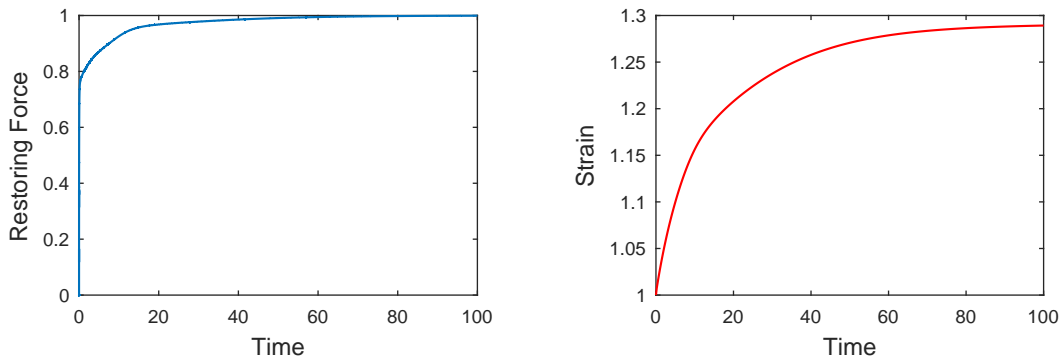


FIGURE 4.11: Left: Restoring force vs time for $\alpha = 0.2$, $\eta = 0.05$, $\lambda = 100$, $\beta = 10$, $\delta = 50$ for the creep experiment using the reference frame and the axiality model described above. Right: Strain vs time for the same experiment.

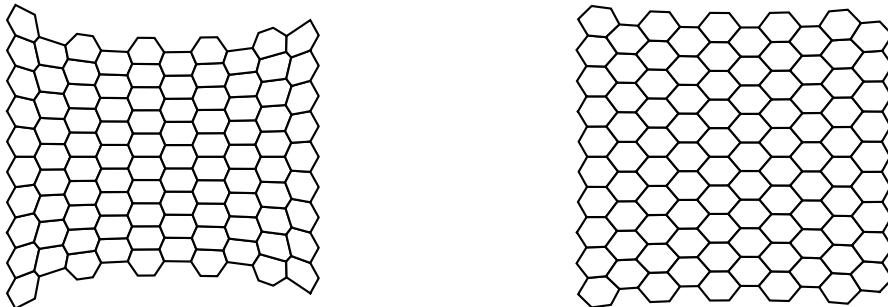


FIGURE 4.12: Final real (left) and reference (right) states for the experiment shown in Figure 4.11.

We can see an example of this model in Figure 4.11. Note we have a monotonic restoring force, as desired. The strain exhibits a relatively rapid increase at low time, followed by a long extension due to the cellular remodelling implemented in the reference state. We can see the reference state in Figure 4.12 exhibiting the appropriate convex behaviour.

However, note that the creep experiment has a preferred direction/axis - between the side held fixed and the side of the monolayer being pulled. More work needs to be done on how such a model responds in a more isotropic system or experiment.

4.8 Vertex Timescales

Due to the increase in model complexity in moving from the cell centre linear spring model to a vertex based model, experiments such as the creep experiment and the stress relaxation experiment do not produce strain-time and stress-time graphs that can be consistently fitted satisfactorily with exponentials or sums of exponentials (e.g. Figure 4.13). Some other fits such as stretched exponentials proved to be marginally better, but not significantly. This proved true even in the base model without the use of the reference state or additions to the model, and adding these effects had the potential to further confuse the fits.

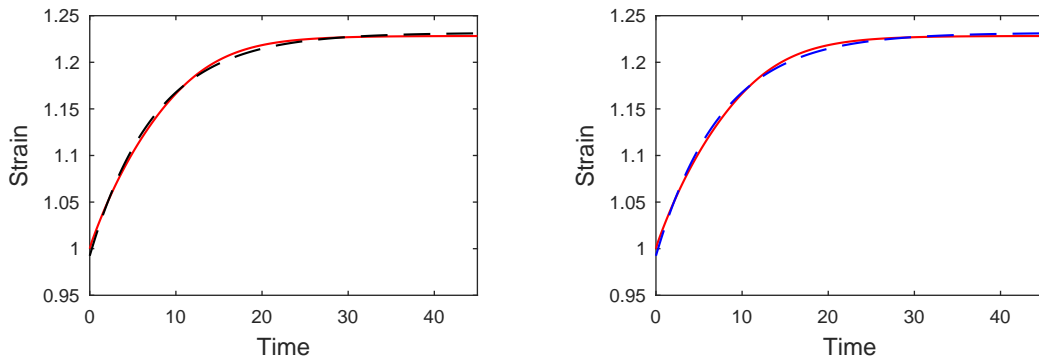


FIGURE 4.13: Creep experiment with no remodelling, with data in red, one exponential fit in black (left) and two exponential fit in blue (right). Note that the two exponential fit cannot improve on the one exponential fit.

Due to this, the detailed analysis that was done in Chapter 3 for the cell centre linear spring model becomes greatly complicated, especially for parameter regimes where there is a less dramatic presence of remodelling, as the analysis there required the use of accurate and consistent fits for the timescale analysis.

We do, however, see the appropriate type of effects that we want, achieving two timescales with appropriate parameters. This can be seen by fitting the graph in Figure 4.11 with exponentials, as seen in Figure 4.14, where we see a significant increase in the quality of the fit by moving to a two exponential fit from a one exponential fit.

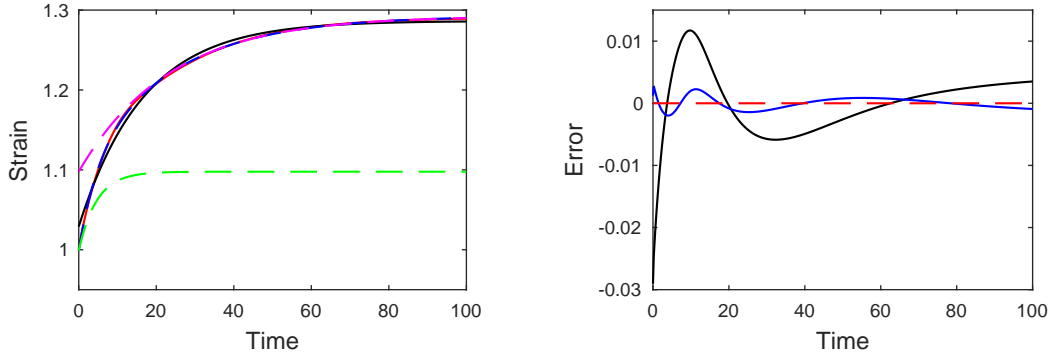


FIGURE 4.14: Left: Fits for the strain-time graph in Figure 4.11. The data is in red, the two exponential fit is blue, the one exponential fit is in black, the short timescale of the two exponential fit is in green and the long timescale of the two exponential fit is in magenta. Right: Error of the one exponential fit (black) and two exponential fit(blue)

For the stress relaxation experiment, even without the presence of remodelling components, we tend to get stress-time graphs that have the appearance of biexponential behaviour. This is likely due to the multiple components acting on the vertices of the cell, with cells attempting to match a target area, circumference, and principal axis length. The effects of this however, can be exacerbated with the presence of cellular remodelling, as shown in Figure 4.15, where the addition of cellular remodelling dramatically increases the long timescale of the system shown in magenta.

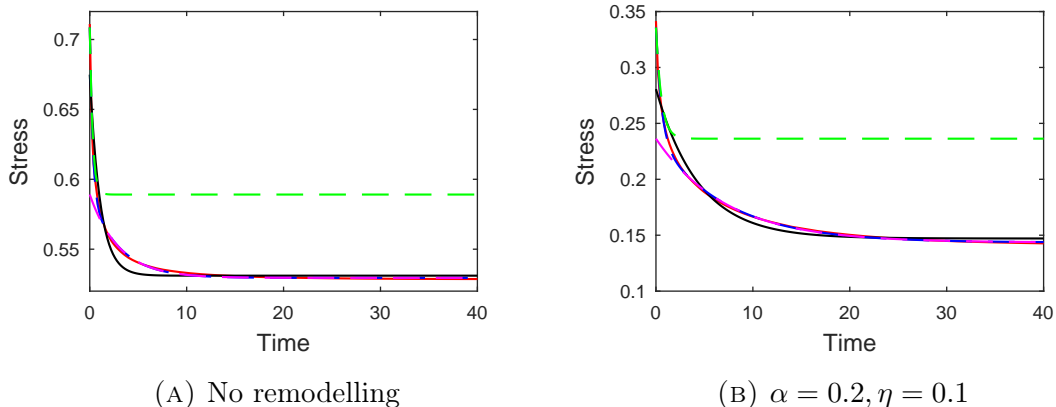


FIGURE 4.15: Stress-time graphs from the stress relaxation experiment, with $\lambda = 100, \beta = 10, \delta = 10$ and a ramptime of 50.

4.9 Summary

After implementing the reference state for a cell centre approach, a similar idea was attempted in order to simulate the remodelling behaviour of cells with a more complicated vertex based approach. Using the success of the idea of varying the target parameters of the cell centre based model, the target area and circumference between the real and reference states were matched in order to implement the remodelling.

Due to the increased complexity of the model in the vertex based approach and the various parameters characterising the size and shape of the cells, this method resulted in unwanted behaviour, including tendencies for cell concavity, and unpredictable relaxation of cells leading to unwanted variation in mechanical behaviour.

In an attempt to ameliorate these effects, the reference state was forced to be roughly regular hexagonal by synchronising the target area and circumference used in the reference state. This idea worked inasmuch that the reference state displayed convex behaviour and unpredictable relaxations of the reference state were avoided. However, a side effect of this synchronisation led to feedback loops, increasing or decreasing the size of certain cells and leading to numerical singularities.

After these implementations of the reference state failed to produce optimal behaviour, the vertex model was augmented with the addition of a component relating the length of the cell along its principal axis. Using this component as the driver of remodelling, our reference state was not prone to concavities or numerical instabilities as in the previous sections. With this, we managed to produce the effects of cellular remodelling, the magnitude and rate of which we can vary by changing the remodelling parameters α and η in order to match empirical behaviour as desired.

Chapter 5

Discussion & Conclusion

5.1 Discussion

5.1.1 Overview

It was noticed experimentally that upon doing mechanical experiments with monolayers, multiple timescales were observed, due to the different biological processes within the cell causing cellular remodelling at different rates. We notice that with existing cell models, the existence of static parameters only allow the dominant biological effects within the cell to be modelled. This generally produces the presence of a singular main timescale, when we discount the presence of factors such as cell growth or intercalation.

In this document, we implemented reference states into both cell centre and vertex based models in an attempt to simulate the presence of different effects of cellular remodelling at different rates in a general manner, which can be observed as multiple timescale behaviour of the monolayers when subjected to creep and stress relaxation experiments.

In the cell centre models, a simple addition of a reference state in the cell centre model produced the desired results, with this effect being noticeable to varying extents depending on the parameters used in the construction of the reference state. The addition of averaging increased the effects of multiple timescale behaviour, but when extreme enough also produced some effects that were not exponential in nature.

Vertex models, due to the nature of their increased complexity of geometry, inherently require more complicated equations of motion in order to describe the behaviour of their defining vertices. Due to this, the addition of the reference state is not so simple as in the cell centre model, with extra components needing to be

added to the vertex model for appropriate behaviour to be observed when we include the reference state.

Because we can control the rate and extent of flow of information between the real and reference states, for a given monolayer we should be able to adjust our model to behave accordingly so that our computational simulations match the experimental data. Therefore, based on either knowledge of the internal restructuring behaviours of the cells or bulk biological data we should be able to adjust the model accordingly for a variety of different cell types and situations.

5.1.2 Computational Overhead

Although we have managed to include additional effects into our model to more accurately reflect biological phenomena, this included the presence of extra calculations which both increases the models complexity and the amount of calculations that need to be done. In all biological simulations, care needs to be taken to determine the relevant features in the simulations, and whether or not any given additional feature should be added to increase simulation complexity at the cost of time. Therefore, a test of a few scenarios with and without the reference state were timed in order see the impact of adding a reference state. This was done with MATLAB's `cputime` function, on an iMac 16.2 with an Intel I5-5575R processor, using the settings described in Appendix E, and all measurements are in seconds.

For the cell centre model, we tested this using the creep experiment, with force on the righthand cells of 1 with and end time of 500, enough to allow all the systems to equilibrate. A remodelling rate of $\eta = 1$ was used.

With no reference state, this creep experiment took 4.16 seconds.

We then add a reference state over varying parameters:

	$\alpha = 1$	$\alpha = 0.5$
T= 0	5.38	16.28
T = 10	5.70	45.04

We see that the addition of a reference state, with no remodelling ($\alpha = 1$) does not massively increase the amount of time it takes to run. In other words, the presence of extra cells that do not end up moving is a relatively low cost on the system. Adding a small amount of averaging does not massively affect the performance of the system either; keeping track of a small amount of intercellular distances is a relatively low cost.

However, when we let remodelling occur ($\alpha = 0.5$), this dramatically increases the time taken for the simulation to run, by a factor of around 3. This is further increased when averaging was introduced, causing another factor of three slowdown. This slowdown is significant, but not cripplingly so. However, as many of the same

two exponential effects could be seen without the need for the averaging parameter, it would generally appear that the cost of adding such an effect is not worth the computational cost.

We can also see the impact of varying these parameters with the vertex model. All simulations are run with $\lambda = 100$, $\beta = 10$, and tests which have the length component have $\gamma = 10$.

No directionality, no remodelling	186.36
Directionality, no remodelling	215.83
Directionality, $\alpha = 0.5$, $\eta = 1$.	402.39

We see a small increase in time needed to simulate the experiment when we add the presence of directionality, and a much more significant effect on the computation when the remodelling was added.

We see that the addition of remodelling, in both settings, includes a significant increase in computational time. Whether or not this increase in computational time is worth it depends on the specific problem; if extra computational time is available, and these cellular remodelling effects are one of the main drivers of tissue movement rather than intercalation or cell growth, then it seems very reasonable that the addition of cellular remodelling would be valuable.

Note that we have been using MATLAB's ODE solvers, rather than the forward Euler scheme used in most cell modelling approaches, which will reduce the time step when needed to ensure accuracy. Because of this, the relative time differences may not stay constant when moving to a different implementation.

5.2 Future Work

5.2.1 Application to Other Discrete Models

One of the main advantages of the use of the reference state is its relative simplicity; because the reference state has very similar properties to the real state, addition of the reference state to these models should be not too difficult, compared to more complicated additions. It should be easily extendable to tessellated cell centre models with different force functions than the linear spring.

Some difficulties were encountered with the implementation of the vertex model, with the naïve implementation encountering some unexpected issues which had to be worked around via the addition of some extra components to the model. One obvious avenue for future work is attempting to modify alternative models, such as the one by Weliky and Oster [43, 44], with a reference state to see the possibilities of changing parameters via a reference state to include the presence of multiple

timescales. Similarly, formulations such as the finite element model seem like possible avenues for generalisation, and models such as the sub-cellular element model also seem to have great potential for the addition of a reference state due to their analogue with standard cell centre models.

With these models, work would need to be done to see exactly how the real and reference states would interplay when different attempts of linking these two states are implemented. The importance of seeing these effects between states can be seen in the implementation of the vertex model, showing that these effects can be more complicated than expected.

5.2.2 Complex System Simulation

All of the work done in this document involves relatively artificial experiments to test the mechanical properties of cell monolayers. Work would need to be done to see the impact of the addition of a reference state and consequently the addition of multiple timescales in “real” simulations. The effects on the overall behaviour of the system that cellular remodelling produces needs to be observed to see whether it better matches experimental data.

5.2.3 Monolayer Restructuring with Reference State

Often we want the connectivity of the cells to change, due to birth or death processes of cells, or rearrangement of cells due to external forces [11]. Birth processes generally involve the division of a mother cell into two daughter cells, requiring the connectivity of the other cells to shift in response to this. Forces acting on cells can cause vertices to become too close, or for cells to intersect, requiring locations and connections to be created or shifted.

A reference state, at least in all of the current formulations, requires the same connectivity between the two states for the appropriate parameter information to be transferred. Therefore, how the reference state reacts to these changes in connectivity is paramount if these operations are implemented.

In response to any change in the real state, evidently any change in connectivity needs to be emulated in the reference state. For example, if one would like to implement mesh restructuring operations such as T1 swaps [11], vertices being too close together in the real state would trigger the T1 swaps of the vertices in the real state and the corresponding vertices in the reference state simultaneously.

However, the method to implement this in the other direction, from reference state to real state, is not immediately clear. In simulations where cells are exposed to a high degree of force, it may be appropriate for the reference state to undergo

cell restructuring operations; see Figure 4.3 for an example of non-convex reference cells where mesh restructuring operations could be applied. However, any change in connectivity would have to be replicated in the real state, potentially in cases where the real state is in no need of such changes.

We surmise that the method of only allowing the changes to move in one direction, from a higher level state (the real state) to a lower one (the reference state), appears to be the best option on paper, due to the lack of physical interpretation for an abstract reference state influencing real cell connectivity. However, work would need to be done to see the impact of differing choices for the restructuring behaviour of vertex models with a reference state, in order to find the optimal choice of model implementation.

5.2.4 Multiple Reference States

In this model, our reference state based its movement on both the position of the real cells, as well as a set of static parameters. However, our reference state could have its own reference state to allow its parameters to change. This would allow the effects of another set of cell components with their own differing remodelling timescales to be implemented, with their own sets of remodelling rates and remodelling ratios.

This process could theoretically be repeated *ad infinitum* (subject to computational constraints), with each reference frame having another reference frame in order to simulate as many timescales, and inherently the presence of biological processes, as necessary in order to accurately model the monolayer behaviour.

5.3 Conclusion

In this document, a novel method of representing cellular remodelling was developed and implemented via the formulation of a reference state. Both cell centre and vertex models were augmented with this reference state, and managed to reproduce remodelling based behaviour of monolayers seen experimentally. The implementation of the reference state was based directly on standard cell centre linear spring approaches, while in vertex based models, additional components representing cytoskeletal length were required in order to observe appropriate behaviour of the model. More work needs to be done to integrate existing model components, such as connectivity changing operations, with the reference state. In addition, avenues of future research include implementing the reference state in other cell based models, and to realise this model in a wider range of biological simulations.

Appendix A

Numerical Calculation of Forces in the Vertex Model

We have described the equations of motions of cells in regards to gradients of physical properties of cells. These need to be converted into forms that be used to numerically calculate the forces acting on the cell vertices. The majority of the resulting expressions can be found in Fletcher et al. [11], with the results in this appendix going into more detail about how these values are calculated.

First, notice that changing the location of a vertex only changes the properties of cells containing that vertex, saving computation time. Let N_i be the set of all cells containing vertex i .

Let A_c^k be the current area of the cell and A_t^k be the target area of the cell in question. Similarly, let C_c^k be the current circumference of the cell and C_t^k be the target circumference of the cell.

The area of cell k , with k_j being the j th vertex counterclockwise of cell k can be represented as:

$$A_c^k = \frac{1}{2} \sum_{j=0}^{n_k-1} x_{k_j} y_{k_{j+1}} - x_{k_{j+1}} y_{k_j}.$$

The circumference is given by the sum of distances between cells:

$$C_c^k = \sum_{j=0}^{n_k-1} \|\mathbf{v}_{k_j} - \mathbf{v}_{k_{j+1}}\|.$$

For the following, let vertex i be the l th vertex of the cell k , counted anticlockwise.

The gradient due to the area component is:

$$\nabla_i \sum_{k \in N_i} \lambda (A_c^k - A_t^k)^2 = \sum_{k \in N_i} 2\lambda (A_c^k - A_t^k) \nabla_i A_c^k.$$

The gradient can be expressed as follows, with vertex i being the vertex k_l :

$$\nabla_i A_c^k = \nabla_i \left(\frac{1}{2} \sum_{j=0}^{n_k-1} x_{k_j} y_{k_{j+1}} - x_{k_{j+1}} y_{k_j} \right) = \frac{1}{2} (y_{k_{l+1}} - y_{k_{l-1}}, x_{k_{l-1}} - x_{k_{l+1}}).$$

For the remaining quantities, their values are based on distances between vertices. The gradient for a vertex i for the distance between cells i and j is given by

$$\begin{aligned} \nabla_i \|\mathbf{v}_i - \mathbf{v}_j\| &= \nabla_i \sqrt{(x_i - x_j)^2 + (y_i - y_j)^2} \\ &= \frac{1}{\sqrt{(x_i - x_j)^2 + (y_i - y_j)^2}} (x_i - x_j, y_i - y_j) \\ &= \frac{\mathbf{v}_i - \mathbf{v}_j}{\|\mathbf{v}_i - \mathbf{v}_j\|} \end{aligned}$$

The gradient due to the circumference is given by

$$\nabla_i \sum_{k \in N_i} \beta (C_c^k - C_t^k)^2 = \sum_{k \in N_i} 2\beta (C_c^k - C_t^k) \nabla_i C_c^k,$$

with

$$\nabla_i C_c^k = \nabla_i \|\mathbf{v}_{k_l} - \mathbf{v}_{k_{l+1}}\| + \nabla_i \|\mathbf{v}_{k_{l-1}} - \mathbf{v}_{k_l}\|.$$

Similarly, the gradient resulting from the intercellular boundary energies is represented as

$$\nabla_i \sum_{j=0}^{n_k-1} \mu_j^k \|\mathbf{v}_{k_{j+1}} - \mathbf{v}_{k_j}\| = \mu_l^k \nabla_i \|\mathbf{v}_{k_{l+1}} - \mathbf{v}_{k_l}\| + \mu_{l-1}^k \nabla_i \|\mathbf{v}_{k_l} - \mathbf{v}_{k_{l-1}}\|.$$

Finally, for the axiality components, let L_c^k be the current length of cell k and L_t^k be the target length of cell k . The gradient due to this component is given by

$$\nabla_i \sum_{k \in N_i} \delta(L_c^k - L_t^k)^2 = \sum_{k \in N_i} 2\delta(L_c^k - L_t^k) \nabla_i L_c^k.$$

Let k_p and k_q denote the vertices in cell k that are furthest apart. The length of the cell is given by the distance between the two furthest vertices, and so therefore

$$L_c^k = \|\mathbf{v}_{k_q} - \mathbf{v}_{k_p}\|.$$

As the force only acts on the two most distant vertices, we get as the value for the gradient for vertex i

$$\begin{aligned} \nabla_i L_c^k &= \nabla_i \|\mathbf{v}_{k_q} - \mathbf{v}_{k_p}\| \\ &= \delta_{l,q} \nabla_i \|\mathbf{v}_{k_l} - \mathbf{v}_{k_p}\| + \delta_{l,p} \|\mathbf{v}_{k_l} - \mathbf{v}_{k_q}\|, \end{aligned}$$

with $\delta_{m,n}$ representing the Kronecker δ function.

In our experiments in this document, there was always a preferred axial direction, the horizontal direction, with both the creep and stress relaxation experiments involving forces and movement in this direction. Therefore, these two furthest axes tended to be the left and rightmost vertices in our simulations.

Appendix B

Implementation Details of Creep and Stress Relaxation Experiments

In both the creep and stress relaxation experiment simulations in the cell centre model, the left hand side of the cell monolayers are held fixed via setting all of the derivatives acting upon these cells to zero. For the right hand, extra care needs to be taken for the *in silico* experiment to match the experiments done in the Harris paper. In these experiments, the sides of the monolayer are fixed to straight rods that are moved or held fixed, depending on the experiment and side. Therefore, the final column of cells on the right hand side of the monolayer are held in fixed relative position to each other.

For the creep experiment, in order to implement this in MATLAB, all vertical forces on this right hand are discarded, effectively being absorbed by the rod the monolayers are connected to. For the horizontal forces, the forces on the cells in the final column are averaged over all of the cells in this column, allowing the relative positions of the cells to stay fixed.

In the stress relaxation experiment, in the initial period where the strain is increasing linearly, the right hand column of cells are moved in concert with each other horizontally in accordance with the strain rate. In the relaxation component of the experiment, these cells are then held fixed. Again, in both stages, the vertical components of the force on these cells are discarded to keep the cells in fixed relative position.

Appendix C

Defining Two Timescaled Behaviour

C.1 Suitability of Stretched Exponential Fits

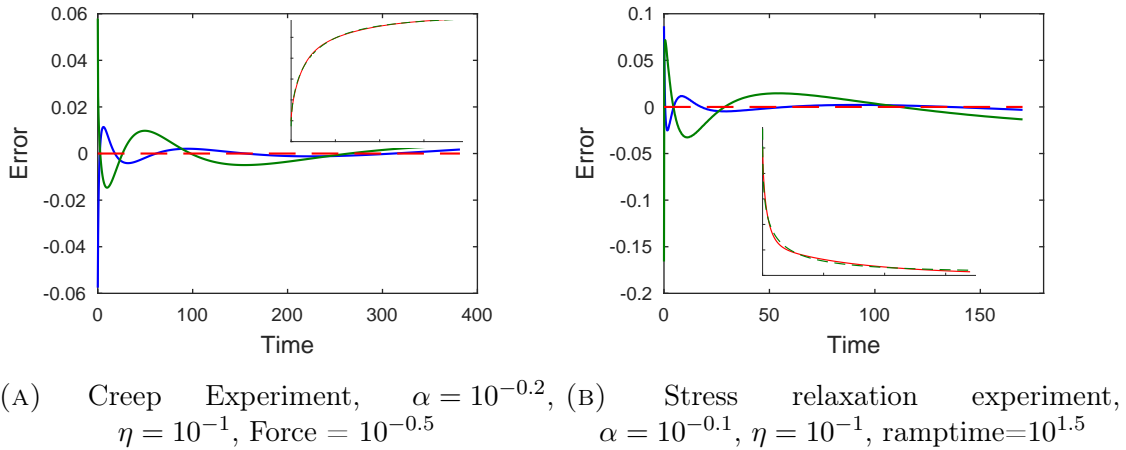


FIGURE C.1: Graphs showing the difference between the two exponential fit and the original data in blue, and difference between the stretched exponential fit and the data in green. Inset is the data overlaid by the stretched exponential fit.

In Figure C.1, we can see that the sum of exponentials fit is significantly better than the stretched exponential fit, for both the creep and stress relaxation experiment. The unsuitability of the stretched exponential also reflects back to the original experimental paper [16], where a stretched exponential fit was attempted, and noticed that it didn't fully fit the data.

C.2 Choice of Metric

We defined regions of multiple timescale behaviour via fitting the graphs with exponentials, and using the ratios of timescales of these fits in order to determine whether or not a simulation exhibited two timescales, with higher values of the coefficient ratio τ_r indicating the greater presence of multiple timescale behaviour. Several other methods were initially attempted before this choice was eventually realised.

Several methods of comparing errors from the fits directly were attempted; for example, dividing the L^2 errors of the one exponential and two exponential fits. Unfortunately, often this method was highly variable, with very small differences in L^2 error for the two exponential fit causing large differences in this ratio.

Other attempts to utilise the L^2 norm and related metrics, such as the infinity norm were attempted but ultimately discarded. For an example of why they were not appropriate, notice that in the two regions within the plots, the one exponential curve will attempt to mostly match the long timescale (as the exponential due to the long timescale is the dominant exponential for the majority of the plot). Due to this, the L^2 error to a large extent measures how well the fit matches to the long timescale, and this becomes more prevalent for low values of η and α .

Due to this, the L^2 error may be appropriate for measuring the difference between plots, but is not an appropriate metric to determine biexponential behaviour. This could be potentially fixed with some kind of weighted measure, where discrepancies in plots at earlier times are weighted more heavily than those at later times in order to have a more equal balance in the contributions from the long and short timescales, but this was not investigated.

Appendix D

Equilibration Time Calculation

The simulations were all run over a very long period of time (two million time units in MATLAB) so that the systems could equilibrate, especially important for lower values of η and α . In order to plot and analyse graphs, an appropriate time interval is needed to compare graphs of different parameters. For the creep experiment, the time it took for 90% of the creep to occur was found, and twice this value was used as the final time.

This was slightly more involved in the stress relaxation experiment. The long term stress is completely determined by the value of α , as this is the only parameter in the system that determines the structure of the system as time approaches infinity; this occurs in both the creep and stress relaxation experiments. In the creep experiment, the initial value of the creep is always one, meaning choosing a 90% point is simple. However, in the stress relaxation experiment, the initial (and maximum) stress is dependent on both η and T . In order to get a non-biased initial value for the stress dependent only on alpha (not η or T), we want an instant remodelling of the system to be used as a reference. This was implemented by running an extra simulation, for each ramptime- α pair, with $T = 0$ and a very high value of η , $\eta = 1000$, three orders of magnitude higher than any values used in the simulation, in order to approach instant remodelling. The initial stress of this simulation was recorded, and two times the 90% point between the initial and final values of stress was used in order to calculate a final time.

Regarding the choice of bounds for η and α , lower values of α and η were originally attempted to be swept over, but computational constraints, such as MATLAB's ODE solvers taking a very long time to solve for these values and MATLAB's fit functions having issues fitting these plots informed the above bounds for the sweeps of α and η .

Decreasing α increases the extent of the remodelling, and decreasing η decreases the speed of the remodelling, so we expect that decreasing either of these parameters

will increase the length of time taken in order to equilibrate, which we can see as in Figure D.1.

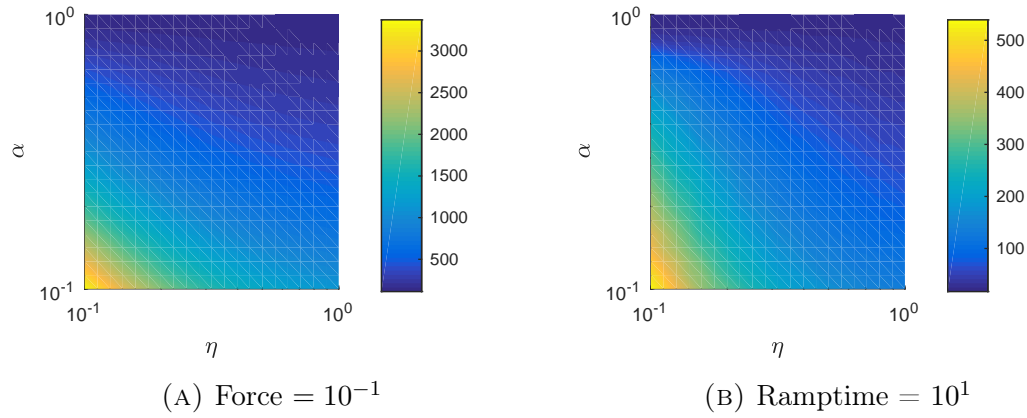


FIGURE D.1: Time to reach equilibrium as a surface plot over η and α for the creep (left) and stress relaxation experiments (right), with no averaging.

Appendix E

Use of MATLAB Solvers for the Solution of ODEs

When solving the ODEs for the equations of motions of the cells, the inbuilt MATLAB ODE solvers were tried, including `ode45`, `ode23` and `ode15s`. The one that was eventually used was `ode15s` for multiple reasons: the solver usually ended up being around five or ten times faster than `ode45`, suggesting that the problem has stiff elements. In addition, `ode45` had the tendency to produce graphs (such as strain or restoring force graphs) with small amounts of jagged elements, while the graphs produced by the `ode15s` solver tended to be smooth.

All simulations shown in this document were therefore run using `ode15s`, with the parameter `RelTol` set as 10^{-5} and `AbsTol` set as 10^{-8} .

We can compare the use of these more complicated solvers to the ones used in other numerical methods for solving biological systems, such as Chaste [24], which uses forward Euler schemes to solve the ODEs. The more complicated methods can be faster depending on the situation, allowing for different time steps to be used as appropriate (which was quite beneficial when doing the parameter sweep, which used a very long time interval to ensure proper equilibration). Variable time solvers also tend to be more accurate than simple forward Euler methods, as they allow smaller time steps to be used in regions of high derivatives.

However, there were some difficulties that were encountered when solving using a non-forward Euler scheme. Calculating average values, such as for area and circumference, were done several times, and in these cases calculating these averages with non-monotonic values of time requires care.

More importantly, however, is the difficulty in calculating restructuring operations to change the connectivities of cells. These operations often require variables (such as the position of a vertex location) to be changed instantaneously or brought into

existence as the result of the mesh changing operation. This can be easily done in a forward Euler setting, but implementing this in MATLAB where all differential equations are solved by inputting a list of derivatives is more difficult.

This can be solved by using events to essentially stop and restart the calculation whenever restructuring operations were necessary. The calculation would be stopped via an event, the operation performed on the state and then restarted with the new values. However, constant stopping and starting of the MATLAB solvers reduces much of the benefit gained from using these over their forward Euler counterparts.

Appendix F

Code

All code used in the simulations is available publicly on GitHub:

https://github.com/reubenvanammers/research_code/tree/master/Code/matlab

This includes the code used to create the cell meshes, internal force calculation for the cells, code used to run the experiments (such as as creep, stress relaxation) and to fit and analyse the resulting curves.

Some open source code was used in this work: a method for checking self-intersection of polygons [2], and a method for fitting exponentials without an initial guess [39].

Bibliography

- [1] G Wayne Brodland. Computational modeling of cell sorting, tissue engulfment, and related phenomena: A review. *Applied Mechanics Reviews*, 57(1):47–76, 2004.
- [2] Antoni J. Canos. Fast and robust self-intersections. <https://au.mathworks.com/matlabcentral/fileexchange/13351-fast-and-robust-self-intersections>, 2006. [Online; accessed 15-September-2017].
- [3] Helen H Chen and G Wayne Brodland. Cell-level finite element studies of viscous cells in planar aggregates. *Journal of Biomechanical Engineering*, 122(4):394–401, 2000.
- [4] Stephen C Cowin and Stephen B Doty. *Tissue Mechanics*. Springer Science & Business Media, 2007.
- [5] Andras Czirok and Dona Greta Isai. Cell resolved, multiparticle model of plastic tissue deformations and morphogenesis. *Physical Biology*, 12(1):016005, 2015.
- [6] B. Delaunay. Sur la sphere vide. *Izv. Akad. Nauk SSSR, Otdelenie Matematicheskii i Estestvennyka Nauk*, 7:793–800, 1934.
- [7] Dirk Drasdo. Buckling instabilities of one-layered growing tissues. *Physical Review Letters*, 84(18):4244, 2000.
- [8] Dirk Drasdo, Stefan Hoehme, and Michael Block. On the role of physics in the growth and pattern formation of multi-cellular systems: What can we learn from individual-cell based models? *Journal of Statistical Physics*, 128(1):287, 2007.
- [9] W. Dütting and Th. Vogelsaenger. Recent progress in modelling and simulation of three-dimensional tumor growth and treatment. *Biosystems*, 18(1):79 – 91, 1985.
- [10] Sara-Jane Dunn, Inke S Näthke, and James M Osborne. Computational models reveal a passive mechanism for cell migration in the crypt. *PLoS One*, 8(11):e80516, 2013.

- [11] Alexander G. Fletcher, James M. Osborne, Philip K. Maini, and David J. Gavaghan. Implementing vertex dynamics models of cell populations in biology within a consistent computational framework. *Progress in Biophysics and Molecular Biology*, 2013.
- [12] Yuan-Cheng Fung. Biomechanics. *Applied Mechanics Reviews*, 38(10):1251–1255, 1985.
- [13] Martin Gardner. Mathematical games: The fantastic combinations of John Conway’s new solitaire game “life”. *Scientific American*, 223(4):120–123, 1970.
- [14] K Garikipati, EM Arruda, K Grosh, H Narayanan, and S Calve. A continuum treatment of growth in biological tissue: the coupling of mass transport and mechanics. *Journal of the Mechanics and Physics of Solids*, 52(7):1595–1625, 2004.
- [15] François Graner and James A Glazier. Simulation of biological cell sorting using a two-dimensional extended Potts model. *Physical Review Letters*, 69(13):2013, 1992.
- [16] Andrew R. Harris, Loic Peter, Julien Bellis, Buzz Baum, Alexandre J. Kablaa, and Guillaume T. Charras. Characterizing the mechanics of cultured cell monolayers. *PNAS*, 2012.
- [17] H. Honda, Y. Ogita, S. Higuchi, and K. Kani. Cell movements in a living mammalian tissue: Long-term observation of individual cells in wounded corneal endothelia of cats. *Journal of Morphology*, 174(1):25–39, 1982.
- [18] Hisao Honda, Masaharu Tanemura, and Tatsuzo Nagai. A three-dimensional vertex dynamics cell model of space-filling polyhedra simulating cell behavior in a cell aggregate. *Journal of Theoretical Biology*, 226(4):439–453, 2004.
- [19] Jesús A Izaguirre, Rajiv Chaturvedi, Chengbang Huang, Trevor Cickovski, J Coffland, G Thomas, Gabor Forgacs, M Alber, G Hentschel, Stuart A Newman, et al. Compucell, a multi-model framework for simulation of morphogenesis. *Bioinformatics*, 20(7):1129–1137, 2004.
- [20] Gareth Wyn Jones and S. Jonathan Chapman. Modeling growth in biological materials. *SIAM Rev.*, 54(1):52–118, February 2012.
- [21] A R Kansal, S Torquato, I V Harsh GR, E A Chiocca, and T S Deisboeck. Simulated brain tumor growth dynamics using a three-dimensional cellular automaton. *Journal of Theoretical Biology*, 203(4):367 – 382, 2000.
- [22] Harvey F. Lodish. *Molecular Cell Biology*. New York : W.H. Freeman and Co., 2013., 2013.

- [23] Frank A Meineke, Christopher S Potten, and Markus Loeffler. Cell migration and organization in the intestinal crypt using a lattice-free model. *Cell Proliferation*, 34(4):253–266, 2001.
- [24] G.R. Mirams, C.J. Arthurs, M.O. Bernabeu, R. Bordas, J. Cooper, A. Corrias, Y. Davit, S-J. Dunn, A.G. Fletcher, D.G. Harvey, M.E. Marsh, J. M. Osborne, P. Pathmanathan, J. Pitt-Francis, J. Southern, N. Zemzemi, and D.J. Gavaghan. Chaste: an open source c++ library for computational physiology and biology. *PLOS Computational Biology*, 9(3), 2013.
- [25] José J Muñoz and Santiago Albo. Physiology-based model of cell viscoelasticity. *Physical Review E*, 88(1):012708, 2013.
- [26] Tatsuzo Nagai and Hisao Honda. A dynamic cell model for the formation of epithelial tissues. *Philosophical Magazine B*, 81, 07 2001.
- [27] Tatsuzo Nagai and Hisao Honda. Wound healing mechanism in epithelial tissues cell adhesion to basal lamina. In *Proceedings of the 2006 WSEAS Int. Conf. on Cellular and Molecular Biology, Biophysics and Bioengineering, Athens, Greece*, pages 111–116, 2006.
- [28] Tatsuzo Nagai and Hisao Honda. Computer simulation of wound closure in epithelial tissues: Cell–basal-lamina adhesion. *Physical Review E*, 80(6):061903, 2009.
- [29] T.J. Newman. Modeling multicellular systems using subcellular elements. *Math. Biosci. Eng.*, 2(3):613–624, 2005.
- [30] Katsushi Owaribe and Hirohisa Masuda. Isolation and characterization of circumferential microfilament bundles from retinal pigmented epithelial cells. *The Journal of Cell Biology*, 95(1):310–315, 1982.
- [31] A A Patel, E T Gawlinski, S K Lemieux, and R A Gatenby. A cellular automaton model of early tumor growth and invasion: The effects of native tissue vascularity and increased anaerobic tumor metabolism. *Journal of Theoretical Biology*, 213(3):315 – 331, 2001.
- [32] P Pathmanathan, J Cooper, A Fletcher, G Mirams, P Murray, J Osborne, J Pitt-Francis, A Walter, and S J Chapman. A computational study of discrete mechanical tissue models. *Physical Biology*, 6(3):036001, 2009.
- [33] Matteo Rauzi, Pascale Verant, Thomas Lecuit, and Pierre-Francois Lenne. Nature and anisotropy of cortical forces orienting drosophila tissue morphogenesis. *Nature Cell Biology*, 10(12):1401, 2008.
- [34] Esra Roan and Christopher M Waters. What do we know about mechanical strain in lung alveoli? *American Journal of Physiology-Lung Cellular and Molecular Physiology*, 301(5):L625–L635, 2011.

- [35] Tim Rudge and Jim Haseloff. A computational model of cellular morphogenesis in plants. *Advances in Artificial Life*, pages 78–87, 2005.
- [36] Sebastian A Sandersius and Timothy J Newman. Modeling cell rheology with the subcellular element model. *Physical Biology*, 5(1):015002, 2008.
- [37] Gernot Schaller and Michael Meyer-Hermann. Multicellular tumor spheroid in an off-lattice Voronoi-Delaunay cell model. *Physical Review E*, 71(5):051910, 2005.
- [38] D. Stekel, J. Rashbass, and E.D. Williams. A computer graphic simulation of squamous epithelium. *Journal of Theoretical Biology*, 175(3):283 – 293, 1995.
- [39] Per Sundqvist. Exponential fit, without start-guess.
<https://au.mathworks.com/matlabcentral/fileexchange/21959-exponential-fit--without-start-guess?focused=5108235&tab=function>, 2009. [Online; accessed 19-December-2016].
- [40] András Szabó and Roeland MH Merks. Cellular Potts modeling of tumor growth, tumor invasion, and tumor evolution. *Frontiers in Oncology*, 3, 2013.
- [41] John von Neumann. The general and logical theory of automata. In *Cerebral Mechanisms in Behavior – The Hixon Symposium*. John Wiley & Sons, 1951.
- [42] DC Walker, J Southgate, G Hill, M Holcombe, DR Hose, SM Wood, S Mac Neil, and RH Smallwood. The epitheliome: agent-based modelling of the social behaviour of cells. *Biosystems*, 76(1):89–100, 2004.
- [43] Michael Weliky, S Minsuk, R Keller, and G Oster. Notochord morphogenesis in *xenopus laevis*: simulation of cell behavior underlying tissue convergence and extension. *Development*, 113(4):1231–1244, 1991.
- [44] Michael Weliky and George Oster. The mechanical basis of cell rearrangement. *Development*, 109(2):373–386, 1990.